Priksz Daniel (Orcid ID: 0000-0002-5818-4557)
Sieme Marcel (Orcid ID: 0000-0002-8253-879X)
*Research Paper*

# Nicotinic-acid derivative BGP-15 improves diastolic function in a rabbit model of atherosclerotic cardiomyopathy

**Running title: BGP-15 improves diastolic function in the rabbit**

Daniel Priksz[1], Nora Lampe[1], Arpad Kovacs[2,3,4], Melissa Herwig[2,3,4], Mariann Bombicz[1], Balazs Varga[1], Tician Wilisicz[1], Judit Szilvassy[7], Aniko Posa[8], Rita Kiss[1], Rudolf Gesztelyi[1], Arnold Raduly[6], Reka Szekeres[1], Marcel Sieme[2,3,4], Zoltan Papp[6], Attila Toth[6], Nazha Hamdani[2,3,4,5], Zoltan Szilvassy[1], Bela Juhasz[1,*]

[1]Department of Pharmacology and Pharmacotherapy, Faculty of General Medicine, University of Debrecen, H-4032 Debrecen, Hungary (priksz.daniel@pharm.unideb.hu; lampenori@gmail.com; bombicz.mariann@pharm.unideb.hu; varga.balazs@pharm.unideb.hu; wilisicz.tician95@gmail.com; kiss.rita@med.unideb.hu; gesztelyi.rudolf@pharm.unideb.hu; szekeres.reka@med.unideb.hu; szilvassy.zoltan@med.unideb.hu)
[2]Department of Molecular and Experimental Cardiology, St. Josef-Hospital, Ruhr University Bochum, D-44801 Bochum, Germany (nazha.hamdani@ruhr-uni-bochum.de, melissa.herwig@ruhr-uni-bochum.de; kovacs.arpad@med.unideb.hu; marcel.sieme@ruhr-uni-bochum.de)
[3]Department of Cardiology, St. Josef-Hospital, Ruhr University Bochum, D-44801 Bochum, Germany
[4]Institute of Physiology Ruhr University Bochum, D-44801 Bochum, Germany
[5]Department of Clinical Pharmacology, Ruhr University Bochum, D-44801 Bochum, Germany
[6]Division of Clinical Physiology, Faculty of Medicine, University of Debrecen, H-4032 Debrecen, Hungary (raduly.arnold@med.unideb.hu; pappz@med.unideb.hu; atitoth@med.unideb.hu)
[7]Department of Otorhinolaryngology and Head-Neck Surgery, University of Debrecen, H-4032 Debrecen, Hungary (szj@med.unideb.hu)
[8]Department of Physiology, Anatomy and Neuroscience, Interdisciplinary Excellence Centre, University of Szeged, H-6726 Szeged, Hungary (paniko@bio.u-szeged.hu)
*Correspondence: Bela Juhasz, Ph.D.;
juhasz.bela@med.unideb.hu;
Tel/fax: +3652427899/56109
Department of Pharmacology and Pharmacotherapy, University of Debrecen,
H-4032 Hungary, Debrecen, Nagyerdei krt. 98.

**Word count** (excluding Title page, Methods, Figure legends and References): **3794**

This article has been accepted for publication and undergone full peer review but has not been through the copyediting, typesetting, pagination and proofreading process which may lead to differences between this version and the Version of Record. Please cite this article as doi: 10.1111/bph.15749

**Acknowledgements:** This work was supported by the GINOP- 2.3.2-15-2016-00043 (D.P., M.B., R.G., R.K., B.V., B.J., A.T., Z.P., Z.Sz.), projects co-financed by the European Union and the European Social Fund. N.H was funded by Die Deutsche Forschungsgemeinschaft (HA 7512/2-1). Project no. TKP2020-IKA-04 has been implemented with the support provided from the National Research, Development and Innovation Fund of Hungary, financed under the 2020-4.1.1-TKP2020 funding scheme, and Ministry of Human Capacities, Hungary (grant 20391-3/2018/FEKUSTRAT (A.P.)).

**Conflict of interest:** none declared.

**Declaration of transparency and scientific rigour**: This Declaration acknowledges that this paper adheres to the principles for transparent reporting and scientific rigour of preclinical research as stated in the BJP guidelines for Natural Products Research, Design and Analysis, Immunoblotting and Immunochemistry, and Animal Experimentation, and as recommended by funding agencies, publishers and other organisations engaged with supporting research.

**Availability of Data**: The data that support the findings of this study are available from the corresponding author upon reasonable request. Some data may not be made available because of privacy or ethical restrictions.

**Author contributions:** D.P., B.J., Z.Sz., N.H., A.T. and Z.P. participated in research design. D.P., N.L., A.K., M.H., M.B., B.V., W.T., A.P., R.G., R.K., J.Sz., A.R. R.Sz., M.S. and B.J. conducted the experiments. D.P., N.L., R.G., R.K., A.K., M.B., A.T. and B.J. performed data analyses. N.L., D.P., T.W., A.K., A.P., N.H., Z.Sz., and B.J. wrote the manuscript. All authors contributed to the final manuscript and approved its submission

**Abbreviations**: HC: hypercholesterolemic; HF: heart failure; HFpEF: heart failure with preserved ejection fraction; DD: diastolic dysfunction; LV: left ventricle; PDE: phosphodiesterase; cGMP: cyclic guanosine monophosphate; 5'-GMP: 5'-guanosine monophosphate; PKG: protein kinase G; PKA: protein kinase A; PLB: phospholamban; SERCA2a: sarco/endoplasmic reticulum $Ca^{2+}$-ATPase; VASP: vasodilator-stimulated phosphoprotein; hsp: heat-shock protein; ECM: extracellular matrix; ELISA: enzyme-linked immunosorbent assay; N2B: titin N2B isoform; N2BA: titin N2BA isoform; N2-Bus: titin cardiac-specific unique sequence N2-Bus; Ser: serine; Thr: threonine; PARP-1: poly(adenosine 5-diphosphate)–ribose]polymerase 1; sGC: soluble guanylate cyclase

**Bullet point summary:**

***What is already known***

- Drug candidate BGP-15 reportedly alleviates signs of heart failure in rodent models
- BGP-15 improves striated muscle function in murine disease models, with an unclear mechanism of action

***What this study adds***

- Acute and chronic BGP-15 administration improved diastolic function via the cGMP-PKG-phospholamban pathway in rabbits
- Chronic BGP-15-treatment decreased cardiomyocyte passive tension and reduced titin-based stiffness, independent of vascular status

***Clinical significance***

- BGP-15 was previously proven to be safe in humans, but cardiac actions were not investigated
- Our results provide a rationale for studies to investigate the agent in human diastolic dysfunction

**Abstract**

*Background and Purpose*: Small molecule BGP-15 has been reported to alleviate signs of heart failure and improve muscle function in murine models. Here, we investigated the acute and chronic effects of BGP-15 in a rabbit model of atherosclerotic cardiomyopathy.

*Experimental Approach*: Rabbits were maintained on standard chow (Control) or atherogenic diet (HC) for 16 weeks. BGP-15 was administered intravenously (once) or orally (for 16 weeks), to assess acute and chronic effects. Cardiac function was evaluated by echocardiography, endothelium-dependent vasorelaxation was assessed, and key molecules of the protein kinase G (PKG) axis were examined by ELISA and Western blot. Passive force generation was investigated in skinned cardiomyocytes.

*Key results*: Both acute and chronic BGP-15 treatment improved the diastolic performance of the diseased heart, however, vasorelaxation and serum lipid markers were unaffected. Myocardial cGMP levels were elevated in the BGP-15-treated group, along with preserved PKG activity and increased phospholamban Ser16-phosphorylation. PDE5 expression decreased in the BGP-15-treated group, and the substance inhibited PDE1 enzyme. Cardiomyocyte passive tension reduced in BGP-15-treated rabbits, the ratio of titin N2BA/N2B isoforms increased, and PKG-dependent N2B-titin phosphorylation elevated in the BGP-15-treated group.

Conclusions and Implications: Here we report that BGP-15-treatment improves diastolic function, reduces cardiomyocyte stiffness, and restores titin compliance in a rabbit model of atherosclerotic cardiomyopathy by increasing the activity of the cGMP-PKG axis. As BGP-15 is proven to be safe, it may have clinical value in the treatment of diastolic dysfunction.

**Keywords**: BGP-15, diastolic dysfunction, hypercholesterolemia, titin, protein kinase G

## 1. Introduction

Metabolic syndrome, atherosclerosis and associated diseases often lead to cardiac dysfunction and later chronic heart failure (HF) (Ponikowski et al., 2016). Major risk factors of HF are hypertension, diabetes mellitus and coronary artery disease (CAD), which is the primer causative factor in 50% of all cases (Roger, 2013). The disease has a relatively poor prognosis, and pharmacological treatment of HF, especially diastolic dysfunction is an unmet need (van Heerebeek & Paulus, 2016).

Diastolic dysfunction (DD) can be characterized by abnormal relaxation of the ventricle, accompanied by hypertrophy, remodeling, increased extracellular matrix (ECM) deposition, and can be accompanied by calcium mishandling. Pathophysiological stimuli causing DD promote subcellular changes, mediated by oxidative stress (Zhazykbayeva, Pabel, Mugge, Sossalla, & Hamdani, 2020). Evidence suggests that oxidative stress-related chronic inflammation plays a crucial role in the pathology of DD and Heart Failure with preserved Ejection Fraction (HFpEF), as comorbidities of the disease (metabolic syndrome, arterial hypertension, renal failure and diabetes mellitus) are all linked to inflammatory processes (Zhazykbayeva et al., 2020). Additively, inflammation causes endothelial dysfunction, that affects nitric oxide (NO) – cyclic guanosine monophosphate (cGMP) – protein kinase G (PKG) signaling. This cascade plays an essential role in cardiac relaxation, by affecting wall stiffness via the regulation of the sarcomeric protein, titin; further, by influencing calcium handling of myocytes (Kruger et al., 2009). In addition, NO-signaling exerts anti-fibrotic and anti-hypertrophic effects by affecting the ECM (Inserte & Garcia-Dorado, 2015; Rainer & Kass, 2016; van Heerebeek et al., 2012). Increased oxidative stress and coronary microvascular endothelial inflammation result in degradation of cGMP, hence reduces PKG activity (Kovacs, Alogna, Post, & Hamdani, 2016). Thus, oxidative stress-related modifications of these key signaling proteins contribute to a decrease in diastolic performance (Breitkreuz & Hamdani, 2015). Protein misfolding induces the transcription of heat-shock proteins, with particular importance of hsp27, hsp70 and hsp90 in the myocardium (Hu, Van Marion, Wiersma, Zhang, & Brundel, 2017; Kotter et al., 2014). The expression of hsp27 is induced during ischemic injury and end-stage failure, while hsp70 is associated with atherosclerosis and hypertension (Vander Heide, 2002; Willis & Patterson, 2010). Pharmacological induction of hsp variants may reduce inflammation-mediated processes, protein misfolding, thereby protect physiological mechanisms essential for cardiac relaxation (Borges et al., 2012; Hu et al., 2017). Heat-shock proteins, in the presence of oxidative stress, may suppress titin-based stiffening of

cardiomyocytes, and hence ameliorate diastolic dysfunction (Herwig et al., 2020; Kotter et al., 2014). Beside reducing oxidative stress, heat shock proteins may directly affect cardiac relaxation and NO-signaling, moreover, induction of hsp70 reduces cardiac fibrosis, and restores skeletal muscle function and strength in dystrophic mice (Gehrig et al., 2012; Kennedy et al., 2016; Pasqua et al., 2015). Inducing heat-shock proteins and enhancing cGMP-PKG signaling are promising strategies against cardiomyocyte remodeling and diastolic dysfunction.

Considering translational aspects, it has recently been proposed that low-dose cholesterol-fed rabbits are suitable models of DD, as they show robust echocardiographic signs of diastolic failure with elevated inflammatory markers and oxidative stress, but preserved systolic function (Nachar et al., 2019; Zhazykbayeva et al., 2020). Cardiac physiology of the rabbit is similar to the human in terms of $Ca^{2+}$ handling, ion channel- and actin-myosin structure (Bers, 2002; Kertesz et al., 2013). New-Zealand rabbits maintained on atherogenic diets for months develop myocardial infarction and HF, however, short-term or low-dose cholesterol feeding only causes dyslipidemia and DD (Kertesz et al., 2013; Priksz et al., 2018; Rubinstein, Pelosi, Vedre, Kotaru, & Abela, 2009). Similar pathophysiological processes have been described in a multi-morbid swine model receiving atherogenic diet and low-dose streptozotocin (Sorop et al., 2018). As these hypercholesterolemic leporine and porcine models might be useful tools for translational studies aimed to better understand the pathophysiology of DD (Nachar et al., 2019; Priksz et al., 2018; Sorop et al., 2018).

Increasing evidence suggests that the nicotinic-acid derivative BGP-15 (3-piperidino-2-hydroxy-1-propyl)-nicotinic amidoxime) improves muscle function and strength, restores cardiac function by attenuating atrial enlargement, and reduces the incidence of arrhythmias in models of muscular dystrophy, HF and diabetic cardiomyopathy (Gehrig et al., 2012; Sapra et al., 2014). BGP-15 may act as an hsp72 co-inducer, increases membrane fluidity, and enhances mitochondrial function, however, the primary mechanism of action is still unclear (Kennedy et al., 2016). Our previous studies demonstrated that BGP-15 improves diastolic function in the diabetic Goto-Kakizaki rat, possibly by increasing the activity of the cardiac PKG enzyme (Bombicz et al., 2019), independently of antidiabetic actions. Downstream mediators of the PKG-pathway transmit anti-hypertrophic signals, furthermore, the PKG-target phospholamban (PLB) and titin proteins are significant regulators of cardiac relaxation (Inserte & Garcia-Dorado, 2015; Kruger et al., 2009; Rainer & Kass, 2016; van Heerebeek et al., 2012). Based on the above, we presume that BGP-15 might have beneficial effects on diastolic function in other models, by influencing the effectors of the PKG pathway. In addition, the hsp-coinducer action of BGP-15 may further contribute to its proposed cardioprotective effects.

This study is aimed to evaluate the effects of BGP-15 in a rabbit model of atherosclerotic cardiomyopathy and diastolic dysfunction, with particular interest regarding the activity of the myocardial cGMP-PKG–titin axis.

## 2. Material and Methods

### 2.1. Animal model and chemicals

The animals received humane care, and all experimental procedures were carried out in accordance with the "Principles of Laboratory Animal Care" by EU Directive 2010/63/EU. All experimental protocols were approved by the local Ethics Committee of University of Debrecen (25/2013DEMÁB and 10/2018/DEMÁB). Animal experiments are reported in compliance with the ARRIVE guidelines and with the recommendations made by the British Journal of Pharmacology (Lilley et al., 2020).

Male adult New Zealand white rabbits (20-22 weeks of age, 2700-3200 g; Charles River Laboratories Inc., Wilmington, MA, USA) were housed under standard conditions (22-24 °C) in the animal house of the Department of Pharmacology and Pharmacotherapy, University of Debrecen, Hungary. The rabbit cage size was 600 mm x 450 mm x 450 mm, with a floor space of 2444 $cm^2$, and each animal were housed separately, in individual cages. Rabbits were kept under a 12-12 h light-dark cycle, ad libitum access to tap water and chow, and a 2-week adaptation period was provided before the experiments. Hypercholesterolemia (atherosclerotic cardiomyopathy) was generated using "atherogenic" diet for 4 months. The components of the rabbit chow were the followings: crude protein (15.51 %), crude fat (3.9 %), crude fiber (17.51 %), calcium (0.90 %), phosphorus (0.66 %), Vitamin A (25.02 mg/Kg), salt (0.18 %). "Atherogenic" chow contained 1 % cholesterol and 5% additional saturated fat, formulated in the Dept. of Pharmaceutical Technology at the University of Debrecen. Cholesterol-fed rabbits properly replicate aspects of human cardiac dysfunction caused by atherosclerotic cardiomyopathy, as these animals show similar echocardiographic signs and molecular pathologies, originating from oxidative stress, inflammation and impaired cardiomyocyte relaxation (Huang et al., 2004; Nachar et al., 2019) .

BGP-15 (Sigma-Aldrich-Merck KGaA, Darmstadt, Germany) was dissolved freshly in distilled water every morning, before administration via oral gavage technique or intravenous (i.v.) bolus (depending on the study protocol). For ex vivo vascular studies, norepinephrine hydrochloride (NE; as Arterenol®), acetylcholine chloride (Ach), and adenosine 5′-triphosphate disodium salt hydrate (ATP) were purchased from Sigma-Aldrich-Merck KGaA

(Darmstadt, Germany). Chemicals were dissolved in modified Krebs-solution: NaCl: 118 mmol/L, KCl: 4.7 mmol/L, $CaCl_2$: 2.5 mmol/L, $NaH_2PO_4$: 1 mmol/L, $MgCl_2$: 1.2 mmol/L, $NaHCO_3$: 24.9 mmol/L, glucose: 11.5 mmol/L, and ascorbic acid: 0.1 mmol/L (dissolved in redistilled water). All other substances, stains and buffer solutions used in molecular biological methods and cardiomyocyte force measurements were ordered from Sigma-Aldrich-Merck KGaA (Darmstadt, Germany) or Abcam Plc. (Cambridge, UK).

### 2.2. Study design

In acute studies (**Protocol I**), twenty rabbits were randomly divided into hypercholesterolemic (HC, n=10; atherogenic diet) and healthy Control (n=10, on standard rabbit chow) groups. HC animals were fed with atherogenic chow (1 % additive cholesterol and 5 % saturated fat) for 16 weeks, before baseline data acquisition. Echocardiography was performed at week 16, followed by a single bolus injection of BGP-15-solution (10 mg/kg in saline, i.v.), into the ear vein. A 20-minute-long period was provided for drug distribution; then echocardiographic imaging was performed again on each rabbit under the influence of BGP-15. Statistical analyses were performed on 4 subgroups, as the follows: (I) Control rabbits at baseline conditions (Control Pre), (II) the same Control animals under the influence of BGP-15 (Control Post BGP-15), (III) HC animals at baseline (HC Pre), and (IV) HC animals after BGP-15 i.v. bolus (HC Post BGP-15). Echocardiographic data were assessed by a blinded expert.

Another population of rabbits were randomized into the groups of the long-term study (**Protocol II**). Healthy Control rabbits (n=10) received standard chow, while the diseased group (HC, n=10) and the BGP-15-treated group (HC+BGP-15, n=10) received atherogenic chow (described above) for 4 months. BGP-15 was given orally (gavage) to the animals in the HC+BGP-15 group (10 mg/kg, in distilled water), every day. Control and HC animals were treated with vehicle. At the endpoint, echocardiography was carried out, followed by blood sample collection. Thoracotomy was performed under deep anesthesia, and the excised thoracic aorta was subjected to ex vivo vascular studies. Heart was carefully placed into ice-cold $Ca^{2+}$-free Krebs buffer, left ventricle tissue samples were cut and immediately frozen in liquid nitrogen and stored for further analyses and isolated cardiomyocyte experiments. Tissue wet/dry weights and tibial lengths were determined. Heart tissue and aortic root samples were stored in 4% formalin solution for histology. All data (obtained from in vivo and molecular biological methods) were analyzed by a blinded reader.

## 2.3. Echocardiography

Echocardiography was performed under ketamine-xylazine anesthesia (35/3 mg/kg, i.m.), after removing the chest hair of rabbits. Data acquisition was accomplished in accordance with the recommendations of the American Society of Echocardiography (Lang et al., 2015; Nagueh et al., 2016). A Vivid E9 sonograph (GE Healthcare, New York, NY, USA) equipped with a sector 12S-D probe was used, and the dataset was recorded from parasternal long-and short axis, and as well as from apical 3 and 4 chamber views. Ejection fraction (EF), fractional shortening (FS), myocardial wall thickness in systole and diastole, left atrial (LA) size, aortic (Ao) diameter, mitral and tricuspid annular plane systolic excursion (MAPSE, TAPSE; respectively) was determined from M-mode recordings. Pulsed wave Doppler (PW) and tissue Doppler (TDI) echocardiography was also carried out, where transmitral E and A wave velocity, E/A ratio and E wave deceleration time (DecT) was measured. Wall motion was defined by TDI e' and a' waves and e'/a' ratios, measured at the mitral and septal annulus, and the E/e' ratio was calculated. Ejection time (ET), isovolumic contraction and relaxation time (IVCT, IVRT, respectively) was determined, and Tei-index (Myocardial Performance Index, MPI) was calculated as IVRT+IVCT/ET. Left ventricle (LV) outflow tract (LVOT) velocities (LVOT V, maximal and mean) and pressure gradients (LVOT PG, maximal and mean) were recorded. Heart rate (HR), stroke volume (SV), cardiac output (CO) and LV mass was calculated. Speckle tracking method was performed offline on recordings obtained from apical long axis (APLAX) and 4 chamber views by using the EchoPAC PC software (ver. 112, GE Healthcare, New York, NY, USA) Q-analysis/2DStrain measurement option. Endocardial wall (region of interest, ROI) was manually traced. Systolic global longitudinal strain (GLS), strain rate (SR) during the isovolumic relaxation period (SR IVR) was determined and E/SRIVR ratio was calculated.

## 2.4. Serum parameters and morphometry

Blood was collected from the marginal ear vein after 12-h fasting at the endpoint. Serum parameters were determined on the Roche Cobas Integrated platform (Roche Diagnostics GmbH, Mannheim, Germany): low-density lipoprotein (LDL), high-density lipoprotein (HDL) apoliporotein A and B (ApoA, ApoB), creatine-kinase (CK), creatine-kinase myocardial band (CK-MB), osteocalcin (**Suppl. Table 3.**).

Organ samples were excised and weighed after thoracotomy. Whole heart and LV were precisely isolated, weighed and normalized to tibial length. LV samples were placed into 4%

formalin solution and stored for histology. Kidney, lung and liver samples were kept overnight at 60°C, after wet/dry tissue ratios were determined. Left ventricle samples were immediately excised after thoracotomy, placed into $Ca^{2+}$-free Krebs buffer, then were rapidly frozen in liquid nitrogen and stored at -80°C for molecular biological analyses and force measurement of cardiomyocytes. Thoracic aorta was excised, washed, and the distal section was subjected to ex vivo vascular assays, whereas the proximal part was stored in 4% formalin solution for staining.

### 2.5. Histology

Left ventricle samples were subjected to Masson's trichrome staining to visualize collagen fibers. Tissue samples were embedded into paraffin, and 5 µm thick sections were made. After deparaffinization, Masson's trichrome staining was carried out based on the protocol provided by the manufacturer (Sigma-Aldrich Co., St. Louis, MO, USA). On the stained slides cytoplasm and muscle fibers appear in red, whereas collagen display blue coloration. Area of the fibrosis was measured using the manual area-tracking function of the Scion Image for Windows software (ver. 4.0.2., Scion Corporation, USA, RRID:SCR_008673), and was expressed as the percentage of the total field-of-view (FOV) area.

Paraffin-embedded sections of thoracic aorta at 5 µm thickness were subjected to Movat pentachrome staining to visualize atherosclerotic plaques. Staining protocol provided by the manufacturer (Abcam Plc., Cambridge, UK) was followed, and the stained slides were analyzed using a light microscope (40x or 100x magnification). Thickness of the intima and media was measured using the length-measuring function of Scion Image for Windows software (ver. 4.0.2., Scion Corporation, USA), and averaged intima/media ratios were then calculated.

### 2.6. Vascular assays

Ex vivo vascular measurements were performed as previously described (Priksz et al., 2018). Briefly, after sacrificing the rabbits, the distal part of the thoracic aorta was excised (n=5/group), and 2 mm-wide rings were cut off. The isolated aortic rings were mounted using a wire instrument in an organ bath system containing Krebs solution oxygenated with 95% O2 and 5% CO2 (36 C; pH = 7.4), at 10 mN resting tension. The isometric contractile force was measured by a transducer (SD-01; Experimetria Ltd., Hungary) connected to workstation with

SPEL Advances Isosys software (SOFT-02; MDE GmbH, Heidelberg, Germany). On the rings, three concentration-response (E/c) curves were constructed (separated by wash-out periods) with norepinephrine (NE), acetylcholine (Ach) and adenosine-5'-triphosphate (ATP). Before the Ach and ATP E/c curves, the aortic rings were pre-contracted at the half-maximal effective concentration (EC50) of NE determined from the NE E/c curve. Responses of aortic rings obtained from the same animal were averaged (4 samples per animal). The effect of NE was defined as an increase of the contractile force in addition to the resting tension (10 mN). The effect of Ach and ATP was defined as a percentage change in the initial tension of the ring.

### 2.7. Force measurement of single cardiomyocytes

Single skinned cardiomyocytes isolated from the LV tissues of the long-term study groups (Control, HC, HC+BGP-15) were subjected to force measurements, as previously described in murine models (Borbely et al., 2009; Hamdani et al., 2013). Briefly, samples were thawed in relaxing solution (containing in mM: 1.0 free $Mg^{2+}$; 100 KCl; 2.0 EGTA; 4.0 Mg-ATP; 10 imidazole; pH 7.0), and cell membranes were removed using 0.2 % Triton-X solution (Sigma-Aldrich-Merck KGa). Single myocytes were isolated using an inverted microscope (Zeiss Axiovert 135, 40x objective; Carl Zeiss AG Corp, Oberkochen, Germany) and attached between a force transducer and a piezoelectric motor (Aurora Scientific, Aurora, Ontario, Canada). Passive force ($F_{passive}$) was recorded over the sarcomere length range of 1.8 to 2.4 μm. Force values were normalized to myocyte cross-sectional area.

### 2.8. Western blot, and the assessment of phospholamban phosphorylation after sGC stimulator treatment

Western blot analyses were carried out as previously described (Bombicz et al., 2019) and in agreement with the guideline of the Journal (S. P. H. Alexander et al., 2018). In brief, 300 mg deep-frozen myocardial tissue samples were used for protein isolation. The powdered tissues were homogenized in a buffer containing 25 mM Tris-HCl, pH = 8, 25 mM NaCl, 4 mM Na-orthovanadate, 10 mM NaF, 10 mM Na-pyrophosphate, 10 nM okadaic acid, 0.5 mM EDTA, 1 mM PMSF and protease inhibitor cocktail (Sigma-Aldrich, St. Louis, MO, USA). Total protein concentration was measured by the QuantiPro™ BCA Assay Kit (Sigma-Aldrich-Merck KGaA, Darmstadt, Germany). Samples were loaded (10 μg total protein/well) and were separated using SDS-polyacrylamide gel electrophoresis (SDS-PAGE), then were transferred onto a nitrocellulose membrane via electro-blotting (at 40 mA for 120 min). After blocking with 3% BSA, membranes were incubated overnight at 4°C with primary antibodies, as the

follows: anti-protein kinase G (PKG, RRID:AB_10679736), anti-sarcoplasmic/endoplasmic reticulum calcium ATPase 2a (SERCA2a, RRID:AB_261442), anti-heat-shock protein 72 (hsp72, RRID:AB_477057), anti-vasodilator-stimulated phosphoprotein (VASP, RRID:AB_2043166), anti-phopsho(Ser239)-vasodilator-stimulated phosphoprotein (p-VASP, RRID:AB_11179348), anti-phosphodiesterase 9A (PDE9A, RRID:AB_1088426), anti-phosphodiesterase 5A (PDE5A, RRID:AB_10604138), anti-phospholamban (PLB, RRID:AB_11133263), anti-phospho(Ser16)-phospholamban (p-PLB, RRID:AB_301562), and anti-glyceraldehyde-3-phosphate-dehydrogenase (GAPDH, RRID:AB_1078991; as a housekeeping protein), obtained from Sigma-Aldrich (Sigma-Aldrich-Merck KGaA and Abcam (Abcam Plc., Cambridge, UK). Antibodies were used in dilutions recommended by the manufacturer; catalog numbers are shown in Suppl. Table 5. Visualization of protein bands were made by horseradish peroxidase-conjugated secondary antibodies and Enhanced Chemiluminescense reagent (RRID:AB_258167, RRID:AB_257896, RRID:AB_258242, WesternBright™, ECL, Advansta Inc., CA, USA). Detection and data analysis were carried out by a C-Digit® blot scanner and the Image Studio Digits ver. 5.2. software (LI-COR Inc., Lincoln, NE, USA). Data was averaged from 2 independent experiments (n=6 samples/group), and protein expression is shown as the percentage of pixel density relative to those of the Control group, which was considered 100 %, to reduce further unwanted sources of variation.

In addition, LV samples from the chronic study groups (n=6/group) were thawed in relaxing solution and incubated in vitro with 1.5 μM sGC stimulator (BAY 41-2272, Sigma-Aldrich) for 30 minutes. After, samples were homogenized in 50 mM Tris-SDS buffer (pH 6.8) containing 8 μg/mL leupeptin (Peptide Institute, Ibaraki, Osaka, Japan) and 10 μL/mL phosphatase inhibitor cocktail (P2850; Sigma-Aldrich). Samples were separated by 15 % SDS-PAGE, transferred onto a polyvinylidene difluoride (PVDF) membranes (Immobilon-P 0.45 μm; Merck Millipore, Burlington, MA, USA) at 25 V. Then, blots were incubated overnight at 4°C with an anti-phospho(Ser16/Thr17) PLB antibody (RRID:AB_10949102, Cell Signaling Technology, Danvers, Massachusetts, USA). After washing with TTBS (tris-buffered saline with 0.1 % Tween 20), a secondary horseradish peroxidase-labeled antibody and enhanced chemiluminescence (ECL Western blotting detection; Amersham, Sigma-Aldrich) were used for visualization. Signals were detected using the LAS-4000 Image Reader and analyzed with Multi Gauge V3.2 software (FUJIFILM, Minato, Tokyo, Japan). The expression of p-PLB was normalized to GAPDH, and datasets of groups (before and after the sGC stimulator treatment) were compared by paired t-test.

## 2.9. Determination of myocardial cGMP-content

Quantification of cGMP level in LV myocardial samples of the rabbits was carried out by a direct competitive immunoassay (Abcam Plc., Cambridge, UK), as described previously (Priksz et al., 2018). After preparing standard absorbance-cGMP concentration curve, samples of animals (n=5/group, measured in duplicates) were homogenized in 0.1M HCl. Measurement protocol recommended by the manufacturer was strictly followed. The amount of horseradish-peroxidase (HRP)-conjugated cGMP, bound to the specific G-protein-covered 96-well plate was measured by determining optical density (OD) at 450 nm, using a plate reader (FLUOstar Optima, BMG Labtech, Ortenberg, Germany). The amount of cGMP in myocardial samples was calculated using the equation described by the manufacturer, and data was expressed as pmol/mg tissue in each group.

## 2.10. In vitro PDE inhibitor screening assay

The ability of BGP-15 (substance, dissolved in distilled water) to inhibit the phosphodiesterase-1 enzyme (PDE1) was determined using a specific colorimetric assay (Abcam Plc., Cambridge, UK). The basis of the assay is the cleavage of cGMP by PDE1 to 5'-GMP, which is further cleaved into GMP and phosphate by the enzyme 5'-nucleotidase, and the phosphate is quantified using Malachite Green reagent. After preparing the standard curve (absorbance - 5'-GMP concentration), wells of a 96-well microplate were loaded with assay buffer, 0.5 mM cGMP substrate, 5'-nucleotidase enzyme (5 kU/ml), PDE1 enzyme (4 mU/µL), and the test compound (BGP-15). BGP-15 was added in concentrations of 40, 100, 200 and 500 µM to "test" wells, respectively. Blank wells contained only the assay buffer (for background subtraction), further, "positive control" wells were loaded with 40 µM isobutyl-1-methylxanthine (IBMX, $IC_{50}$ for PDE1 = 25 µM). "Control" wells contained the reaction mixture without any drug. After incubation at 37°C for 50 mins, a modified Malachite Green assay reagent was added to each well, the reaction ended, and the green color was able to develop for 20 mins. Absorbance was measured using a Varioskan LUX spectrometer (ThermoFisher Scientific Inc., Waltham, MA, USA) at 620 nm, and the amounts of the generated 5'-GMP were calculated. PDE1 activity in "test" wells were normalized to "Control" PDE1 activity, which was considered 100 %. Data was analyzed using one-way ANOVA with Tukey post-test.

### 2.11. Titin assays

Analysis of titin isoform composition and titin phosphorylation assays were carried out as previously described (Hamdani et al., 2013; Kotter et al., 2013). Briefly, LV tissue samples were solubilized in 50 mM Tris-SDS buffer (pH 6.8) containing 8 μg/mL leupeptin (Peptide Institute, Ibaraki, Osaka, Japan) and 10 μL/mL phosphatase inhibitor cocktail (P2850; Sigma-Aldrich). Samples were heated for 3 min at 96°C and centrifuged, and were applied in duplicates at concentrations that were within the linear range of the detection system, and separated by agarose-strengthened 1.8% SDS-PAGE (4 mA constant current for 16 hours). Thereafter, Western blot was performed to measure site-specific and total phosphorylation of titin. Following SDS-PAGE, proteins were transferred to PVDF membranes (Immobilon-P 0.45 μm; Merck Millipore, Burlington, MA, USA). Blots were pre-incubated with 3% bovine serum albumin in Tween Tris-buffered saline (TTBS; containing: 10 mM Tris-HCl; pH 7.6; 75 mM NaCl; 0.1% Tween; all from Sigma-Aldrich) for 1 h at room temperature. Then, blots were incubated overnight at 4°C with the primary antibodies. Anti-phospho-serine (Ser)/threonine (Thr) antibody (RRID:AB_1184778, ECM Biosciences, Versailles, KY, USA; dilution 1:500) was used to assess total titin phosphorylation. Furthermore, a custom-made, affinity-purified phospho-serine-specific antibody (Eurogentec, Seraing, Belgium) against phospho-Ser4080 of murine N2B-titin was used to exclusively show PKG-dependent titin phosphorylation (Linke & Hamdani, 2014). After washing with TTBS, antibody binding was visualized using secondary horseradish peroxidase-labeled antibody (RRID:AB_2617138, DakoCytomation, Glostrup, Denmark; dilution 1:10,000) and enhanced chemiluminescence (ECL Western blotting detection; Amersham). Signals were visualized using the LAS-4000 Image Reader and analyzed with Multi Gauge V3.2 software (FUJIFILM, Minato, Tokyo, Japan). Coomassie-based PVDF stains were saved for comparison of protein load and to assess titin N2BA/N2B isoforms ratio.

### 2.12. Statistical procedures and data analysis

The statistical analyses fulfil the recommendations of the British Journal of Pharmacology on experimental design and analysis in pharmacology (Curtis, Ashton, Moon, & Ahluwalia, 2018). All experiments were designed to generate groups of equal size using randomization and blinded analysis. Data presented as the mean value of the group ± standard error of the mean (SEM), unless stated otherwise. In Protocol I, baseline echocardiographic parameters were compared to the same parameters recorded 20 minutes after BGP-15

administration, both in healthy Control (n=10) and hypercholesterolemic (HC; n=10) rabbits. To determine how the responses are affected by the two factors (the BGP-15 treatment and the atherogenic diet), two-way repeated measure ANOVA (2-way-RM-ANOVA) with Sidak's multiple comparison test was performed on longitudinal data across two time points, and interaction of the two factors was also calculated (Figure 2). In Protocol II, to compare endpoint parameters (in vivo, ex vivo, and in vitro data) of 3 groups, Gaussian distribution was estimated by Shapiro-Wilk normality test. Statistical analysis then was performed using one-way analysis of variance (ANOVA) followed by Tukey post-test (only if F in ANOVA achieved $p < 0.05$, normality test was passed, and there was no significant variance inhomogeneity), or Kruskal-Wallis test followed by Dunn's post-test (when normality test was not passed). Statistical analyses were carried out using GraphPad Prism software for Windows, version 7.00 (GraphPad Software Inc., La Jolla, CA, USA; RRID:SCR_002798). Statistical analyses were carried out only for experiments where each group size was at least n=5. Group numbers were determined based on the minimum numbers required for statistical analyses, also considering our previous studies and possible losses due to the treatments. No data points or outliers were excluded from the analyses. Probability values (p) less than 0.05 were considered significantly different and marked with an asterisk (*: $p<0.05$). Group sizes are defined as the follows: n = number of animals, or independent samples originating from individual animals; and N = number of independent cardiomyocytes. Group sizes represent the number of independent samples/animals, not technical replicates. When two or more samples were examined from one source, the values were averaged, and the mean value was subjected to statistical analyses. The term "fold control mean" indicates that each raw value has been divided by the value of the mean of the controls.

### 2.13. Nomenclature of proteins and ligands

Key protein targets and ligands in this article are hyperlinked to corresponding entries in http://www.guidetopharmacology.org, and are permanently archived in the Concise Guide to PHARMACOLOGY 2021/22 (S. P. Alexander et al., 2021).

## 3. Results

### 3.1. Both single-dose and long-term BGP-15 treatment improve diastolic function in HC rabbits

Echocardiographic effects of single-dose i.v. BGP-15 were evaluated using HC rabbits at the 16$^{th}$ week of atherogenic diet and age-matched healthy Controls. Baseline (drug-free) data from both groups were compared to data obtained after BGP-15 (i.v. bolus) injection, using 2-way RM ANOVA (**Figure 1-2**). (Adjusted p values were also calculated by Sidak multiple-comparison test in HC Pre vs. HC Post-BGP-15 groups; **Suppl. Table 4.).**

In single-dose studies (Protocol I, **Figure 2a-h**), Control and HC animals differed in baseline echocardiographic values. E/A and e'/a' ratios were decreased in HC animals after the atherogenic treatment. E/e' ratio and Tei-index was increased in HC rabbits, but Ejection Fraction (EF) only moderately decreased, in accordance with the data obtained from the long-term study group population (Protocol II), and our previous findings in a similar rabbit model (Priksz et al., 2018). EF was unaltered in both study groups after BGP-15-injection. Drug administration decreased heart rate (2-way RM-ANOVA). BGP-15 treatment increased E/A ratio, but only in HC rabbits (HC pre vs. HC Post BGP-15, Sidak MC). Tissue Doppler (TDI) e' wave velocity and e'/a' ratios were increased after BGP-15 administration in both groups, but the changes were more prominent in HC animals (HC Pre vs. HC Post BGP-15; Sidak MC). The E/e' ratio (indicative for LV filling pressure) decreased after the BGP-15 bolus in both groups (2-way RM-ANOVA), but the change again was more distinct in HC animals (HC Pre vs. HC Post-BGP-15, Sidak). Tei-index decreased significantly in HC animals.

In long-term studies (Protocol II, 10 mg/kg BGP-15 per os, for 16 weeks), echocardiographic changes showed similarities with those of single-dose studies (**Figure 3a-g, Suppl. Table 1.**). A left atrial enlargement (LA/Ao ratio) was shown in HC group compared to Control (pControl *vs.* HC), which was counteracted by the chronic BGP-15 treatment (HC+BGP-15 *vs.* HC). Wall thickness values, MAPSE and TAPSE were unchanged. More prominent changes were found in diastolic function, as E/A and tissue e'/a' ratios were decreased in the HC group, and Deceleration Time (DecT) lengthened; while these values of BGP-15-treated rabbits were improved compared to HC. E/e' ratio increased in HC group (HC vs. Control), while decreased in HC-BGP-15 vs. HC. The same pattern was observed in isovolumic relaxation time and Tei-index (**Suppl. Table 1.**). Thus, both single-dose and chronic BGP-15 treatment significantly improved echocardiographic parameters, particularly the diastolic function.

### 3.2. Morphometric parameters of rabbits were unaffected by BGP-15

No significant differences were found in morphometric parameters of rabbits in the long-term study groups (**Suppl. Table 2.).** Rabbits in HC and HC+BGP-15 groups gained weight, as a result of the diet. Heart weight slightly increased in the treated rabbits, but the weight of the left ventricle (normalized to the tibial length) was similar among the groups. Echocardiography-derived morphometric parameters LV mass index (LVMI), LV end-diastolic volume index (LVEDVi), and relative wall thickness (RWT%) improved only tendentiously in the BGP-15 treated animals compared to HC. Masson's trichrome stain revealed mild fibrotic remodeling in both HC and HC+BGP-15 groups, but the extent of fibrosis was decreased in the HC+BGP-15 groups compared to HC (**Figure 3h-i**). Tissue wet to dry ratios did not differ significantly between groups.

### 3.3. BGP-15 treatment did not influence serum lipid parameters of rabbits

Severe dyslipidemia developed in HC rabbits after 16 weeks of atherogenic diet. Total cholesterol, LDL, HDL, ApoA and ApoB levels increased in both HC and HC+BGP-15 groups compared to the Control (**Suppl. Table 3.**). BGP-15 treatment failed to improve serum lipid parameters, liver enzymes or CK and CK-MB levels. Levels of serum osteocalcin (a marker that negatively correlates with coronary heart disease (Sheng et al., 2013; Y. Zhang et al., 2010), decreased in both HC and HC+BGP-15 samples compared to Control.

### 3.4. BGP-15 treatment did not alter the endothelium-dependent vasorelaxation and vascular status in aortic samples of HC rabbits

The response to NE of aortic rings isolated from rabbits differed significantly between the Control and HC groups at 10 and 100 nmol/L NE concentrations (**Figure 4a**). In all groups, Ach elicited first (≤ 1 μmol/L) an arterial relaxation, and at higher concentrations (> 1 μmol/L), it caused contraction. Atherogenic diet attenuated the relaxing action of Ach (Control vs. HC). BGP-15 treatment did not affect the endothelial dysfunction (**Figure 4b**). ATP caused an arterial relaxation in all groups, which was stronger in the Control group than in both the HC and HC+BGP-15 groups. In agreement with the results obtained with Ach, BGP-15 did not alter the influence of the atherogenic diet on vasorelaxation (**Figure 4c**).

Movat staining revealed atherosclerotic plaque coverage in the intimal surface of HC and HC+BGP-15 groups, while the aortic samples of the Control group were free from lesions. The mean intima/media ratio (**Figure 4d**) increased in the HC group vs. Control, and slightly

decreased in the HC+BGP-15 group compared to HC. Despite, aortic root cross-sections of the HC+BGP-15 group still showed atherosclerotic plaque coverage.

### 3.5. BGP-15 treatment decreased skinned cardiomyocyte passive force in HC rabbits

As diastolic performance of the heart is determined by myofilaments, single skinned cardiomyocytes isolated from the LV samples of the long-term study groups (Protocol II) underwent force measurements. The sarcomere length – tension relationship, expressed as passive force was recorded at sarcomere lengths from 1.8 to 2.4 μm. Passive force at sarcomere length 2.2 - 2.4 μm was significantly greater in the HC group compared to Control. In contrast, myofilament stiffness significantly reduced in the samples harvested from the BGP-15-treated group in comparison to HC, and even compared to those of the Control group (at sarcomere length 2.3 - 2.4 μm; **Figure 5a**).

### 3.6. Myocardial cGMP levels elevated in samples of BGP-15-treated animals

Myocardial cGMP levels were determined in LV tissue samples of animals in the Control, HC and HC+BGP-15 groups. Cyclic GMP levels of Control and HC animals did not differ significantly (10.93±1.304 vs.13.27±1.183 pmol/mg of tissue, in Control and HC, respectively), while cGMP levels in BGP-15-treated animals significantly increased (33.78±4.083 pmol/mg of tissue), in comparison to those of HC samples (**Figure 5b**).

### 3.7. BGP-15 inhibits the PDE1 enzyme in vitro

A phosphodiesterase activity assay was performed to assess the ability of BGP-15 to inhibit the enzyme. Without inhibition (Control), 20 mU PDE enzyme generated 2 nmoles of 5'GMP from 200 μM cGMP at 37 °C in 60 minutes. A non-specific PDE inhibitor, IBMX (3-isobutyl-1-methylxanthine; 40 μM) significantly decreased PDE activity to 67% (vs. Control). BGP-15 dose-dependently inhibited PDE activity comparably to IBMX, which was significant (compared to Control) in concentrations of 100 μM and 200 μM (**Figure 6h-i**).

### 3.8. BGP-15 treatment restored the activity of the protein kinase G axis

Western blot analyses revealed the deterioration of the PKG pathway in the LV myocardium of HC animals, while chronic BGP-15 treatment altered the expression levels of key mediators. PKG expression was significantly elevated in both HC and HC+BGP-15 groups

compared to Control (**Figure 5c**). The cGMP/PKG ratio was lower in the HC group compared to Control, but was elevated in HC+BGP-15 group compared to HC (**Figure 5d**). The ratio of p-(Ser239)-VASP/VASP (indicative for PKG enzyme activity) showed a decrease (Control vs. HC), and was restored in the BGP-15-treated group (HC vs. HC+BGP-15; **Figure 5e**). Although the total expression level of phospholamban decreased in the HC+BGP-15 groups compared to HC (**Figure 6d**), the expression of SERCA, or the PLB/SERCA ratio did not show marked differences between the groups (**Figure 6c**). Phosphorylation of phospholamban at Ser16 (relative to total PLB; p-(Ser16)-PLB/PLB) significantly increased in the HC+BGP-15 group in comparison to HC (**Figure 6e**).

PLB Ser16/Thr17 phosphorylation was decreased in HC samples compared to Control and HC+BGP-15. Treatment of the samples with an sGC stimulator (BAY 41-2272) could not further increase PLB Ser16/Thr17 phosphorylation in the Control, but the sGC stimulator was able to significantly increase PLB phosphorylation in the HC group, showing that PLB was initially dephosphorylated in the diseased animals. On the contrary, the sGC stimulator failed to further increase PLB phosphorylation in the HC+BGP-15 samples, showing that PLB was highly phosphorylated in the BGP-15 treated rabbits (**Figure 6g**).

Expression of PDE9A was elevated in both HC and HC+BGP-15 groups compared to the Control (**Figure 6b**). The expression of PDE5A was elevated in HC group (vs. Control), but decreased in the HC+BGP-15 group compared to HC (**Figure 6a**). The expression of hsp72 did not show marked differences among groups. For all proteins of interest, bands were first normalized to GAPDH as a housekeeping protein, and signal intensities were shown as a percentage of Control (which was considered 100%).

### 3.9. BGP-15 altered titin isoform ratio and increased PKG-dependent titin phosphorylation in HC animals

Analysis of titin isoform composition revealed that the ratio of the stiffer N2B titin isoform significantly elevated in the HC group compared to Control; while decreased in the HC+BGP-15 group compared to HC (**Figure 5f**). A reduced phosphorylation of N2B-titin was detected in the HC samples, and the level of total N2B-titin phosphorylation was significantly higher in the HC+BGP-15 group compared to HC (**Figure 5g**). PKG-dependent Ser4080 phosphorylation of N2B-titin significantly increased in the LV samples of BGP-15-treated

rabbits (vs. HC), in accordance with the increased myocardial cGMP levels and PKG activity (**Figure 5h**).

## 4. Discussion

Here, we comprehensively analysed the mechanisms involved in the beneficial effect of BGP-15 on the cardiac function of rabbits suffering atherosclerotic cardiomyopathy.

Both single-dose and long-term BGP-15-treatment improved diastolic performance. Transmitral E/A ratio of HC rabbits elevated after BGP-15 injection, and E/e' ratio decreased. Tissue e'/a' ratio increased, suggesting that BGP-15 directly affects myocardial relaxation. Although HR slightly decreased in both Control and HC groups, we note that animals were anaesthetized during the echocardiography, thus, evaluating the chronotropic effect of BGP-15 merits further investigations. Chronically BGP-15-treated animals also showed diastolic improvement, described by decreased E/e' ratio and Tei-index; normalized DecT, IVRT, and e'/a' ratios. Systolic parameters showed less marked differences: EF in the HC group remained in the normal range, confirming that a short-term atherogenic diet rather affects diastolic function. Systolic strain (GLPS) tended to decrease in HC animals, and increased in HC+BGP-15. Single-dose BGP-15 treatment did not alter EF in Control or HC rabbits, however, EF slightly elevated in the chronic group. This rabbit model of atherosclerotic cardiomyopathy is characterized by a robust diastolic, but not systolic dysfunction, accompanied by the deterioration of the cGMP-PKG pathway, and increased cardiomyocyte stiffness. However, as signs of edema were not present, we agree that this model does not fulfill the criteria of HFpEF, but, it's a useful tool to mimic diastolic dysfunction pathology.

At the subcellular level, deterioration of the cGMP-PKG pathway essentially contributes to diastolic dysfunction via multiple mechanisms (Bishu et al., 2011; van Heerebeek et al., 2012). We found increased PKG expression in the HC myocardium (which is possibly a compensatory upregulation), however, PKG activity (indicated by p-VASP/VASP and cGMP/PKG ratios) was impaired, in accordance with previous findings obtained on different models of DD (Kolijn et al., 2020; Matyas et al., 2017; van Heerebeek et al., 2012). As a novel finding, chronic BGP-15 treatment elevated myocardial cGMP levels, hence PKG activity. In the heart, cGMP may be generated by sGC, triggered by NO, or by natriuretic peptide receptors (Kuhn, 2015). Inflammatory processes in atherosclerosis cause endothelial dysfunction in coronary microvasculature, diminished NO bioavailability and disrupted PKG signaling, which promotes fibrosis and myocyte stiffness (Sorop et al., 2018; Westermann et al., 2011). We found impaired endothelium-dependent vasorelaxation in HC rabbits, which failed to improve

in the BGP-15 treated rabbits, even though cardiac function recovered. These findings raise the question about the potential molecular target of BGP-15 in the myocardial and vascular tissues. As BGP-15 did not improve lipid parameters (Suppl. Tabl. 3.), atherosclerosis, and vasorelaxation, we hypothesize that it failed to enhance NO bioavailability in the seriously diseased vessel walls. One can speculate that the drug exerts tissue-specific actions, or its effects may be dose-dependent, as the cGMP-PKG pathway has different effectors in the vascular smooth muscle and the myocardium (Kolijn et al., 2020; Tsai & Kass, 2009). This question merits further investigation, regarding that albeit BGP-15 administration enhanced cGMP-signaling in the heart, serum- or vascular cGMP levels were not measured here. Nonetheless, we determined myocardial levels of PDE5A and PDE9A, and the activity of the PDE1 enzyme – regulators of the cGMP level in the heart (Chen, Knight, & Yan, 2018; Rainer & Kass, 2016). We found increased PDE9A and PDE5A expression in the LV samples of HC rabbits, but a decreased PDE5A expression in chronically BGP-15-treated animals, moreover, PDE activity assay showed that BGP-15 inhibits PDE1 enzyme above 40 µM concentration, comparably to specific inhibitors. Consequently, the elevated myocardial cGMP levels and PKG activity in response to chronic BGP-15 treatment may be a result of the decreased PDE5 expression and PDE1 activity in the long-term study group. Nevertheless, diastolic function also improved in the single-dose experiments, but the 20-minute distribution time was not sufficient for protein expression changes. This fact gives particular importance to our mechanistic results, that further support the role of the altered phosphorylation of myofilament proteins and other PKG-targets in the myocardium.

Among PKG substrates, phospholamban (PLB) expression was investigated. PLB contributes to the prolonged relaxation of myocytes via the inhibition of the SERCA pump (MacLennan & Kranias, 2003). When PLB is phosphorylated by PKG or PKA on Ser16/Thr17, its inhibitory effect on the SERCA pump is relieved (Q. Zhang, Scholz, He, Tse, & Weiss, 2005). Total PLB expression decreased in the samples of BGP-15-treated animals, moreover, the ratio of Ser16 PLB increased. This corroborates our *in vivo* data, as we showed that BGP-15 normalized relaxation time (IVRT) of HC rabbits. SERCA expression level and PLB/SERCA ratio did not show significant changes here. Nonetheless, the actions of BGP-15 on the expression of regulatory proteins responsible for calcium homeostasis remain controversial in the literature. Although SERCA and PLB expressions were found to be unaltered by BGP-15 in dystrophic mice, others found elevated SERCA2a gene expression in BGP-15-treated murine hearts (Kennedy et al., 2016; Sapra et al., 2014). Besides the dysregulated $Ca^{2+}$ homeostasis, alterations in ECM synthesis also contributes to DD (Zile &

Brutsaert, 2002). Here, Masson's trichrome staining revealed fibrotic remodeling in the LV samples of the HC group, which was reduced in the HC+BGP-15 group, in accordance with previous findings (Sapra et al., 2014).

Changes in myofilament function were also investigated. A key finding of our study is that chronic BGP-15 treatment reduces diastolic tension in HC cardiomyocytes. As DD is associated with myofilament remodeling, reducing passive stiffness may recover cardiac function (Borbely et al., 2009; Hamdani et al., 2008; Kotter et al., 2013). The diastolic improvement of HC rabbits is presumably explained by the reduced cardiomyocyte stiffness, as a response to the BGP-15-treatment, as the passive tension in the skinned cardiomyocytes decreased significantly in the BGP-15-treated rabbits. Hence, BGP-15 application seems to counteract increased stiffness of myocytes, an elementary feature of DD. As an underlying mechanism, we showed that BGP-15 induces favorable changes in phosphorylation state and isoform composition of titin, a sarcomeric giant protein that could directly determine diastolic tension (Kotter et al., 2013; Zile & Brutsaert, 2002). The stiff N2B and the compliant N2BA titin isoforms are co-expressed in the heart, and a low ratio of N2BA/N2B is associated with a high passive tension. Titin-based stiffness also vary by phosphorylation: both PKA and PKG can phosphorylate the titin N2-Bus, increase its compliance, hence decrease passive stiffness (Kruger et al., 2009). We found that the cardiac titin N2BA/N2B ratio shifted towards the stiff N2B form, moreover, titin N2-Bus phosphorylation tended to decrease in the samples of the diseased (HC) animals, accordant to the increased stiffness. Our findings correspond to data obtained from a recently described hypercholesterolemic swine model (Sorop et al., 2018). Accordant to the functional results, we demonstrated that titin isoform composition and total N2B-titin phosphorylation was restored in the samples of BGP-15-treated animals. Moreover, BGP-15 elevated titin N2B phosphorylation on the Ser4080, the cGMP-PKG-dependent phosphorylation site, which is known to reduce titin-based stiffness (Linke & Hamdani, 2014).

Nevertheless, as a limitation, we could not define the exact mechanism of action of BGP-15, however, our finding that BGP-15 inhibits the PDE1 enzyme partly explains our mechanistic results. This action might be concentration-dependent, but we did not determine the tissue or serum levels of the drug in this current study, as the initial dose was calculated from previous human experiments (Literati-Nagy et al., 2009). The agent was first introduced as an hsp70 co-inducer (Literati-Nagy et al., 2009), however, we failed to demonstrate such an action here. Despite, BGP-15 provided cardiac protection in the absence of hsp70 in a HF+AF-hsp70-knockout model, and it was proposed that it acts via the modulation of membrane fluidity (Sapra et al., 2014). Otherwise, BGP-15 seems to inhibit PARP-1, and modulates

mitochondrial ROS production, which may also contribute to its effects (Peto et al., 2020; Sarszegi et al., 2012). Moreover, BGP-15 was found to block the c-Jun N-terminal kinase, which may also subsidize diastolic improvement (Sarszegi et al., 2012). BGP-15 was shown to reduce symptoms of HF in murine models, improves strength and increases SERCA pump expression in skeletal muscles, however, the primary action mechanism was not elucidated. Our novel findings suggest that BGP-15 treatment increases cardiac cGMP levels, enhances PKG activity, thus, increases the PKG-dependent phosphorylation of titin and phospholamban. These processes led to improved myofilament function and decreased passive stiffness of cardiomyocytes, consequently, improved diastolic function. The links between the mechanistic processes described here and the previously proposed actions of the drug remain elusive; and, together with the limitations of this report, may be addressed in future investigations. Since BGP-15 is proven to be safe in humans, our results may provide a rationale for translational studies aimed to investigate the effects of the drug in diastolic dysfunction.

**References**


Alexander, S. P., Fabbro, D., Kelly, E., Mathie, A., Peters, J. A., Veale, E. L., … Wong, S. S. (2021). THE CONCISE GUIDE TO PHARMACOLOGY 2021/22: Enzymes. *Br J Pharmacol, 178 Suppl 1*, S313-S411. doi:10.1111/bph.15542

Alexander, S. P. H., Roberts, R. E., Broughton, B. R. S., Sobey, C. G., George, C. H., Stanford, S. C., … Ahluwalia, A. (2018). Goals and practicalities of immunoblotting and immunohistochemistry: A guide for submission to the British Journal of Pharmacology. *Br J Pharmacol, 175*(3), 407-411. doi:10.1111/bph.14112

Bers, D. M. (2002). Cardiac Na/Ca exchange function in rabbit, mouse and man: what's the difference? *J Mol Cell Cardiol, 34*(4), 369-373. doi:10.1006/jmcc.2002.1530

Bishu, K., Hamdani, N., Mohammed, S. F., Kruger, M., Ohtani, T., Ogut, O., … Redfield, M. M. (2011). Sildenafil and B-type natriuretic peptide acutely phosphorylate titin and improve diastolic distensibility in vivo. *Circulation, 124*(25), 2882-2891. doi:10.1161/CIRCULATIONAHA.111.048520

Bombicz, M., Priksz, D., Gesztelyi, R., Kiss, R., Hollos, N., Varga, B., … Juhasz, B. (2019). The Drug Candidate BGP-15 Delays the Onset of Diastolic Dysfunction in the Goto-Kakizaki Rat Model of Diabetic Cardiomyopathy. *Molecules, 24*(3)doi:10.3390/molecules24030586

Borbely, A., Falcao-Pires, I., van Heerebeek, L., Hamdani, N., Edes, I., Gavina, C., … Paulus, W. J. (2009). Hypophosphorylation of the Stiff N2B titin isoform raises cardiomyocyte resting tension in failing human myocardium. *Circ Res, 104*(6), 780-786. doi:10.1161/CIRCRESAHA.108.193326

Borges, T. J., Wieten, L., van Herwijnen, M. J., Broere, F., van der Zee, R., Bonorino, C., & van Eden, W. (2012). The anti-inflammatory mechanisms of Hsp70. *Front Immunol, 3*, 95. doi:10.3389/fimmu.2012.00095

Breitkreuz, M., & Hamdani, N. (2015). A change of heart: oxidative stress in governing muscle function? *Biophys Rev, 7*(3), 321-341. doi:10.1007/s12551-015-0175-5

Chen, S., Knight, W. E., & Yan, C. (2018). Roles of PDE1 in Pathological Cardiac Remodeling and Dysfunction. *J Cardiovasc Dev Dis, 5*(2)doi:10.3390/jcdd5020022

Curtis, M. J., Ashton, J. C., Moon, L. D. F., & Ahluwalia, A. (2018). Clarification of the basis for the selection of requirements for publication in the British Journal of Pharmacology. *Br J Pharmacol, 175*(18), 3633-3635. doi:10.1111/bph.14443

Gehrig, S. M., van der Poel, C., Sayer, T. A., Schertzer, J. D., Henstridge, D. C., Church, J. E., … Lynch, G. S. (2012). Hsp72 preserves muscle function and slows progression of severe muscular dystrophy. *Nature, 484*(7394), 394-398. doi:10.1038/nature10980

Hamdani, N., Kooij, V., van Dijk, S., Merkus, D., Paulus, W. J., Remedios, C. D., … van der Velden, J. (2008). Sarcomeric dysfunction in heart failure. *Cardiovasc Res, 77*(4), 649-658. doi:10.1093/cvr/cvm079

Hamdani, N., Krysiak, J., Kreusser, M. M., Neef, S., Dos Remedios, C. G., Maier, L. S., … Linke, W. A. (2013). Crucial role for Ca2(+)/calmodulin-dependent protein kinase-II in regulating diastolic stress of normal and failing hearts via titin phosphorylation. *Circ Res, 112*(4), 664-674. doi:10.1161/CIRCRESAHA.111.300105

Herwig, M., Kolijn, D., Lodi, M., Holper, S., Kovacs, A., Papp, Z., … Hamdani, N. (2020). Modulation of Titin-Based Stiffness in Hypertrophic Cardiomyopathy via Protein Kinase D. *Front Physiol, 11*, 240. doi:10.3389/fphys.2020.00240

Hu, X., Van Marion, D. M. S., Wiersma, M., Zhang, D., & Brundel, B. (2017). The protective role of small heat shock proteins in cardiac diseases: key role in atrial fibrillation. *Cell Stress Chaperones, 22*(4), 665-674. doi:10.1007/s12192-017-0799-4

Huang, Y., Walker, K. E., Hanley, F., Narula, J., Houser, S. R., & Tulenko, T. N. (2004). Cardiac systolic and diastolic dysfunction after a cholesterol-rich diet. *Circulation, 109*(1), 97-102. doi:10.1161/01.CIR.0000109213.10461.F6

Inserte, J., & Garcia-Dorado, D. (2015). The cGMP/PKG pathway as a common mediator of cardioprotection: translatability and mechanism. *Br J Pharmacol, 172*(8), 1996-2009. doi:10.1111/bph.12959

Kennedy, T. L., Swiderski, K., Murphy, K. T., Gehrig, S. M., Curl, C. L., Chandramouli, C., … Lynch, G. S. (2016). BGP-15 Improves Aspects of the Dystrophic Pathology in mdx and dko Mice with Differing Efficacies in Heart and Skeletal Muscle. *Am J Pathol, 186*(12), 3246-3260. doi:10.1016/j.ajpath.2016.08.008

Kertesz, A., Bombicz, M., Priksz, D., Balla, J., Balla, G., Gesztelyi, R., … Juhasz, B. (2013). Adverse impact of diet-induced hypercholesterolemia on cardiovascular tissue homeostasis in a rabbit model: time-dependent changes in cardiac parameters. *Int J Mol Sci, 14*(9), 19086-19108. doi:10.3390/ijms140919086

Kolijn, D., Pabel, S., Tian, Y., Lodi, M., Herwig, M., Carrizzo, A., … Hamdani, N. (2020). Empagliflozin improves endothelial and cardiomyocyte function in human heart failure with preserved ejection fraction via reduced pro-inflammatory-oxidative pathways and protein kinase Galpha oxidation. *Cardiovasc Res*doi:10.1093/cvr/cvaa123

Kotter, S., Gout, L., Von Frieling-Salewsky, M., Muller, A. E., Helling, S., Marcus, K., … Kruger, M. (2013). Differential changes in titin domain phosphorylation increase myofilament stiffness in failing human hearts. *Cardiovasc Res, 99*(4), 648-656. doi:10.1093/cvr/cvt144

Kotter, S., Unger, A., Hamdani, N., Lang, P., Vorgerd, M., Nagel-Steger, L., & Linke, W. A. (2014). Human myocytes are protected from titin aggregation-induced stiffening by small heat shock proteins. *J Cell Biol, 204*(2), 187-202. doi:10.1083/jcb.201306077

Kovacs, A., Alogna, A., Post, H., & Hamdani, N. (2016). Is enhancing cGMP-PKG signalling a promising therapeutic target for heart failure with preserved ejection fraction? *Neth Heart J, 24*(4), 268-274. doi:10.1007/s12471-016-0814-x

Kruger, M., Kotter, S., Grutzner, A., Lang, P., Andresen, C., Redfield, M. M., … Linke, W. A. (2009). Protein kinase G modulates human myocardial passive stiffness by phosphorylation of the titin springs. *Circ Res, 104*(1), 87-94. doi:10.1161/CIRCRESAHA.108.184408

Kuhn, M. (2015). Cardiac actions of atrial natriuretic peptide: new visions of an old friend. *Circ Res, 116*(8), 1278-1280. doi:10.1161/CIRCRESAHA.115.306325

Lang, R. M., Badano, L. P., Mor-Avi, V., Afilalo, J., Armstrong, A., Ernande, L., … Voigt, J. U. (2015). Recommendations for cardiac chamber quantification by echocardiography in adults: an update from the American Society of Echocardiography and the European Association of

Cardiovascular Imaging. *J Am Soc Echocardiogr, 28*(1), 1-39 e14. doi:10.1016/j.echo.2014.10.003
Lilley, E., Stanford, S. C., Kendall, D. E., Alexander, S. P. H., Cirino, G., Docherty, J. R., … Ahluwalia, A. (2020). ARRIVE 2.0 and the British Journal of Pharmacology: Updated guidance for 2020. *Br J Pharmacol, 177*(16), 3611-3616. doi:10.1111/bph.15178
Linke, W. A., & Hamdani, N. (2014). Gigantic business: titin properties and function through thick and thin. *Circ Res, 114*(6), 1052-1068. doi:10.1161/CIRCRESAHA.114.301286
Literati-Nagy, B., Kulcsar, E., Literati-Nagy, Z., Buday, B., Peterfai, E., Horvath, T., … Koranyi, L. (2009). Improvement of insulin sensitivity by a novel drug, BGP-15, in insulin-resistant patients: a proof of concept randomized double-blind clinical trial. *Horm Metab Res, 41*(5), 374-380. doi:10.1055/s-0028-1128142
MacLennan, D. H., & Kranias, E. G. (2003). Phospholamban: a crucial regulator of cardiac contractility. *Nat Rev Mol Cell Biol, 4*(7), 566-577. doi:10.1038/nrm1151
Matyas, C., Nemeth, B. T., Olah, A., Torok, M., Ruppert, M., Kellermayer, D., … Radovits, T. (2017). Prevention of the development of heart failure with preserved ejection fraction by the phosphodiesterase-5A inhibitor vardenafil in rats with type 2 diabetes. *Eur J Heart Fail, 19*(3), 326-336. doi:10.1002/ejhf.711
Nachar, W., Merlet, N., Maafi, F., Shi, Y., Mihalache-Avram, T., Mecteau, M., … Tardif, J. C. (2019). Cardiac inflammation and diastolic dysfunction in hypercholesterolemic rabbits. *PLoS One, 14*(8), e0220707. doi:10.1371/journal.pone.0220707
Nagueh, S. F., Smiseth, O. A., Appleton, C. P., Byrd, B. F., 3rd, Dokainish, H., Edvardsen, T., … Waggoner, A. D. (2016). Recommendations for the Evaluation of Left Ventricular Diastolic Function by Echocardiography: An Update from the American Society of Echocardiography and the European Association of Cardiovascular Imaging. *J Am Soc Echocardiogr, 29*(4), 277-314. doi:10.1016/j.echo.2016.01.011
Pasqua, T., Filice, E., Mazza, R., Quintieri, A. M., Carmela Cerra, M., Iannacone, R., … Angelone, T. (2015). Cardiac and hepatic role of r-AtHSP70: basal effects and protection against ischemic and sepsis conditions. *J Cell Mol Med, 19*(7), 1492-1503. doi:10.1111/jcmm.12491
Peto, A., Kosa, D., Feher, P., Ujhelyi, Z., Sinka, D., Vecsernyes, M., … Bacskay, I. (2020). Pharmacological Overview of the BGP-15 Chemical Agent as a New Drug Candidate for the Treatment of Symptoms of Metabolic Syndrome. *Molecules, 25*(2)doi:10.3390/molecules25020429
Ponikowski, P., Voors, A. A., Anker, S. D., Bueno, H., Cleland, J. G., Coats, A. J., … Document, R. (2016). 2016 ESC Guidelines for the diagnosis and treatment of acute and chronic heart failure: The Task Force for the diagnosis and treatment of acute and chronic heart failure of the European Society of Cardiology (ESC). Developed with the special contribution of the Heart Failure Association (HFA) of the ESC. *Eur J Heart Fail, 18*(8), 891-975. doi:10.1002/ejhf.592
Priksz, D., Bombicz, M., Varga, B., Kurucz, A., Gesztelyi, R., Balla, J., … Juhasz, B. (2018). Upregulation of Myocardial and Vascular Phosphodiesterase 9A in A Model of Atherosclerotic Cardiovascular Disease. *Int J Mol Sci, 19*(10)doi:10.3390/ijms19102882
Rainer, P. P., & Kass, D. A. (2016). Old dog, new tricks: novel cardiac targets and stress regulation by protein kinase G. *Cardiovasc Res, 111*(2), 154-162. doi:10.1093/cvr/cvw107
Roger, V. L. (2013). Epidemiology of heart failure. *Circ Res, 113*(6), 646-659. doi:10.1161/CIRCRESAHA.113.300268
Rubinstein, J., Pelosi, A., Vedre, A., Kotaru, P., & Abela, G. S. (2009). Hypercholesterolemia and myocardial function evaluated via tissue doppler imaging. *Cardiovasc Ultrasound, 7*, 56. doi:10.1186/1476-7120-7-56
Sapra, G., Tham, Y. K., Cemerlang, N., Matsumoto, A., Kiriazis, H., Bernardo, B. C., … McMullen, J. R. (2014). The small-molecule BGP-15 protects against heart failure and atrial fibrillation in mice. *Nat Commun, 5*, 5705. doi:10.1038/ncomms6705
Sarszegi, Z., Bognar, E., Gaszner, B., Konyi, A., Gallyas, F., Jr., Sumegi, B., & Berente, Z. (2012). BGP-15, a PARP-inhibitor, prevents imatinib-induced cardiotoxicity by activating Akt and suppressing JNK and p38 MAP kinases. *Mol Cell Biochem, 365*(1-2), 129-137. doi:10.1007/s11010-012-1252-8

Sheng, L., Cao, W., Cha, B., Chen, Z., Wang, F., & Liu, J. (2013). Serum osteocalcin level and its association with carotid atherosclerosis in patients with type 2 diabetes. *Cardiovasc Diabetol, 12*, 22. doi:10.1186/1475-2840-12-22

Sorop, O., Heinonen, I., van Kranenburg, M., van de Wouw, J., de Beer, V. J., Nguyen, I. T. N., … Duncker, D. J. (2018). Multiple common comorbidities produce left ventricular diastolic dysfunction associated with coronary microvascular dysfunction, oxidative stress, and myocardial stiffening. *Cardiovasc Res, 114*(7), 954-964. doi:10.1093/cvr/cvy038

Tsai, E. J., & Kass, D. A. (2009). Cyclic GMP signaling in cardiovascular pathophysiology and therapeutics. *Pharmacol Ther, 122*(3), 216-238. doi:10.1016/j.pharmthera.2009.02.009

van Heerebeek, L., Hamdani, N., Falcao-Pires, I., Leite-Moreira, A. F., Begieneman, M. P., Bronzwaer, J. G., … Paulus, W. J. (2012). Low myocardial protein kinase G activity in heart failure with preserved ejection fraction. *Circulation, 126*(7), 830-839. doi:10.1161/CIRCULATIONAHA.111.076075

van Heerebeek, L., & Paulus, W. J. (2016). Understanding heart failure with preserved ejection fraction: where are we today? *Neth Heart J, 24*(4), 227-236. doi:10.1007/s12471-016-0810-1

Vander Heide, R. S. (2002). Increased expression of HSP27 protects canine myocytes from simulated ischemia-reperfusion injury. *Am J Physiol Heart Circ Physiol, 282*(3), H935-941. doi:10.1152/ajpheart.00660.2001

Westermann, D., Lindner, D., Kasner, M., Zietsch, C., Savvatis, K., Escher, F., … Tschope, C. (2011). Cardiac inflammation contributes to changes in the extracellular matrix in patients with heart failure and normal ejection fraction. *Circ Heart Fail, 4*(1), 44-52. doi:10.1161/CIRCHEARTFAILURE.109.931451

Willis, M. S., & Patterson, C. (2010). Hold me tight: Role of the heat shock protein family of chaperones in cardiac disease. *Circulation, 122*(17), 1740-1751. doi:10.1161/CIRCULATIONAHA.110.942250

Zhang, Q., Scholz, P. M., He, Y., Tse, J., & Weiss, H. R. (2005). Cyclic GMP signaling and regulation of SERCA activity during cardiac myocyte contraction. *Cell Calcium, 37*(3), 259-266. doi:10.1016/j.ceca.2004.10.007

Zhang, Y., Qi, L., Gu, W., Yan, Q., Dai, M., Shi, J., … Hong, J. (2010). Relation of serum osteocalcin level to risk of coronary heart disease in Chinese adults. *Am J Cardiol, 106*(10), 1461-1465. doi:10.1016/j.amjcard.2010.07.013

Zhazykbayeva, S., Pabel, S., Mugge, A., Sossalla, S., & Hamdani, N. (2020). The molecular mechanisms associated with the physiological responses to inflammation and oxidative stress in cardiovascular diseases. *Biophys Rev*doi:10.1007/s12551-020-00742-0

Zile, M. R., & Brutsaert, D. L. (2002). New concepts in diastolic dysfunction and diastolic heart failure: Part II: causal mechanisms and treatment. *Circulation, 105*(12), 1503-1508. doi:10.1161/hc1202.105290

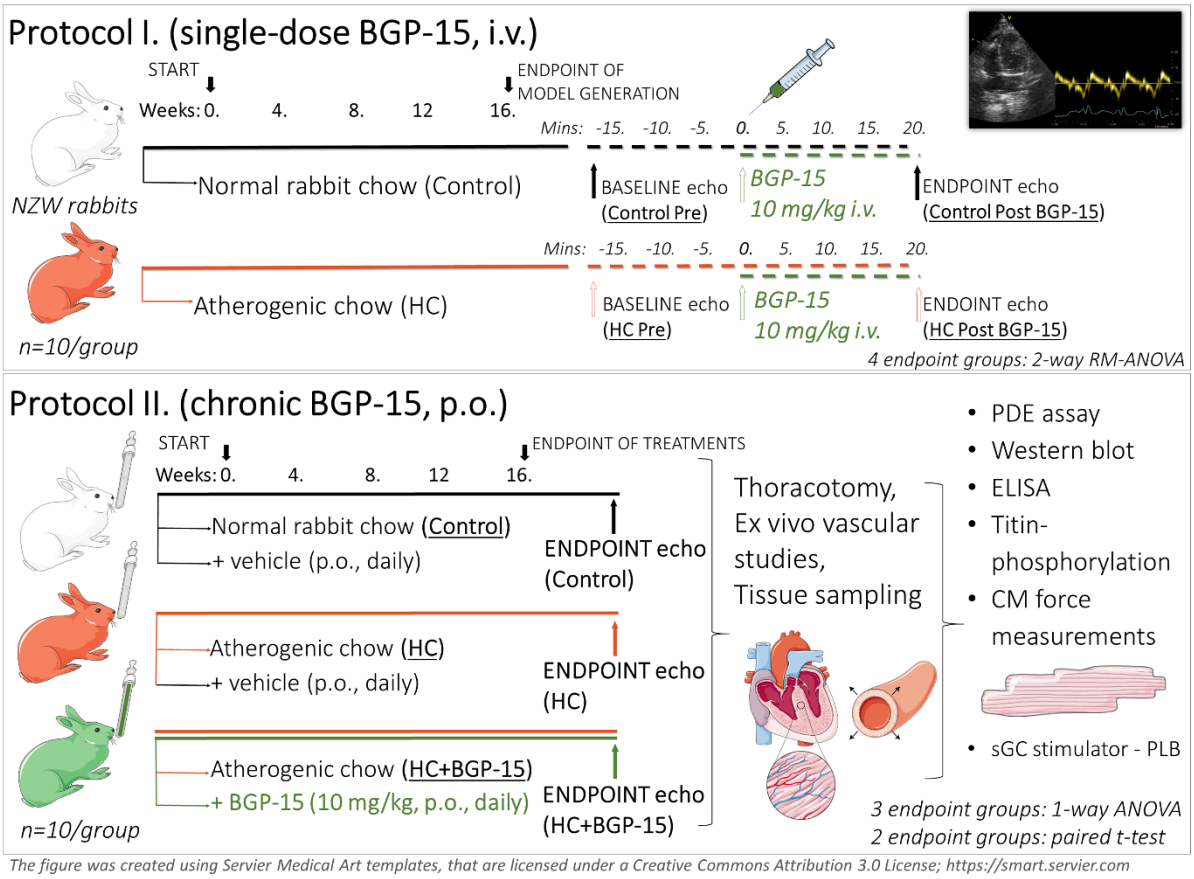


**Figure 1.** Study design. In the single-dose studies (Protocol I), echocardiographic effects of one i.v. bolus BGP-15 was tested in healthy Control and 16-week-hypercholesterolemic (HC) rabbits. Statistical testing of longitudinal data of the two groups (Control vs. HC), across two time points (before and after BGP-15 i.v. administration), was carried out by performing two-way repeated measures (RM) ANOVA. Chronic studies (Protocol II) were carried out on healthy Control, HC and BGP-15-treated HC animals, for 16 weeks. Oral BGP-15 treatment was initiated at the beginning of the atherogenic diet. Parameters of the three endpoint groups were compared by one-way ANOVA and Tukey post-test. The figure was created using Servier Medical Art templates, that are licensed under a Creative Commons Attribution 3.0 License; https://smart.servier.com. HC: hypercholesterolemic; NZW: New-Zealand White; ANOVA: analysis of variance; i.v.: intravenous; p.o.: per os; ELISA: enzyme-linked immunosorbent assay; echo: echocardiography; CM: cardiomyocyte; sGC: soluble guanylyl cyclase; PLB: phospholamban

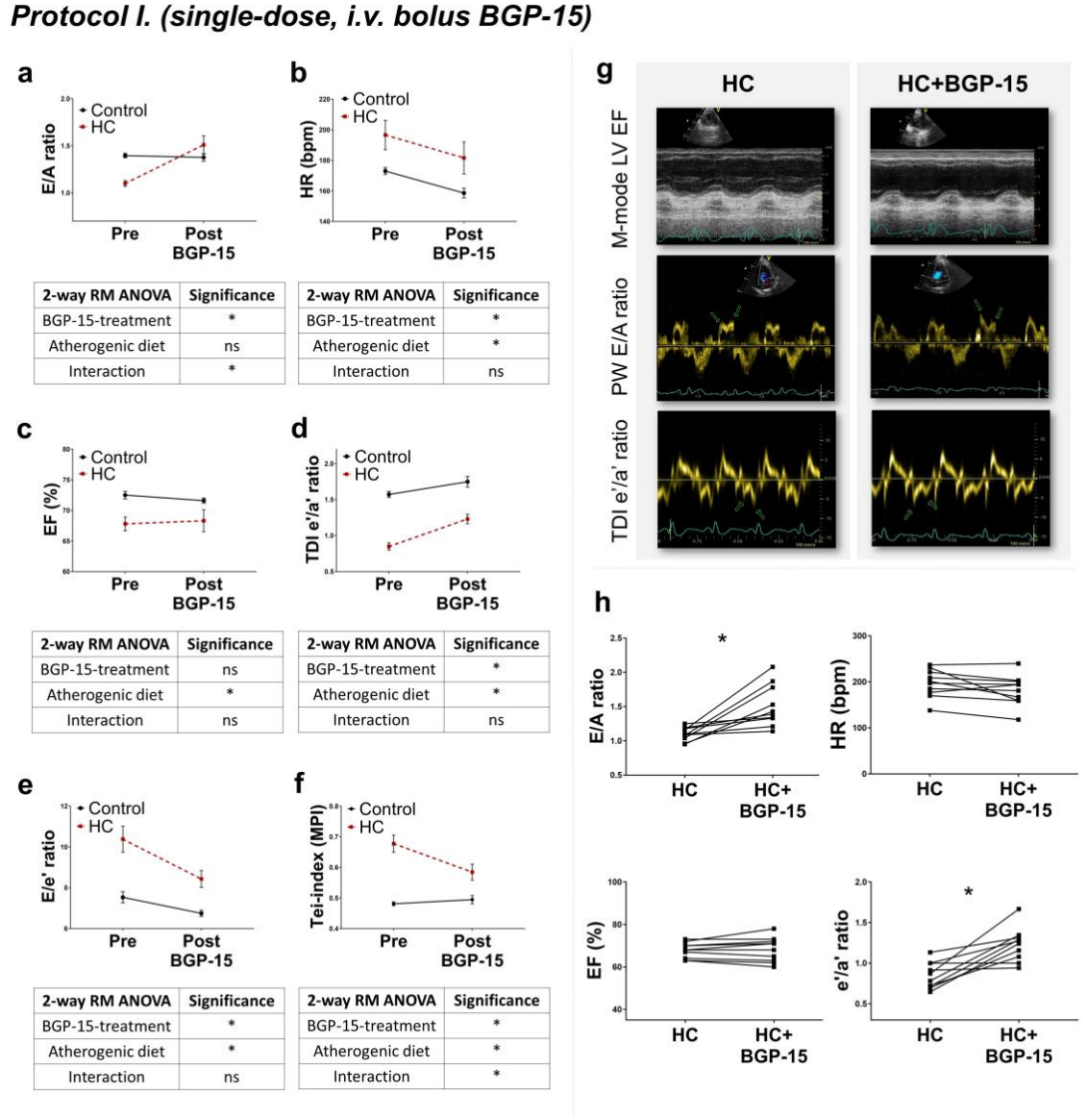


**Figure 2.** The effect of single-bolus BGP-15 on the echocardiographic parameters of Control and HC rabbits. Tables from **a-f** below the graphs show the results of 2-way-repeated measure ANOVA analyses. Groups are Control (n=10), HC (n=10) before (Pre) and 20 mins after (Post BGP-15) the i.v. BGP-15 injection. (**a**) BGP-15 injection restored E/A ratio in HC animals. (**b**) Heart rate (HR) decreased in Control and HC animals after BGP-15 treatment. (**c**) Ejection fraction (EF) did not change under the influence of BGP-15. (**d**) Tissue Doppler (TDI) e'/a' ratio elevated after BGP-15 injection. (**e**) E/e' ratio decreased after BGP-15 bolus, particularly in HC animals. (**f**) Tei-index improved in HC animals after acute BGP-15 treatment. Data presented as mean±SEM; *: $p<0.05$ denotes significance; ns: non-significant; 2-way RM ANOVA). (**g**) Original echocardiography traces of M-mode (parasternal long-axis view), transmitral pulsed wave (PW) Doppler (apical 4-chamber view) and tissue Doppler (TDI, apical 4-chamber view) from HC animals before and after BGP-15 administration (10 mg/kg, i.v.). Green arrows show the pulsed Doppler (PW) transmitral E, A, and tissue Doppler (TDI) septal e', and a' waves, respectively. (**h**) Graphs show the representative scatter of raw data before (HC) and after (HC+BGP-15) the i.v. BGP-15 injection, only in the HC group (n=10). Graphs show: E/A ratio, heart rate (HR), ejection fraction (EF) and tissue e'/a' ratio, respectively. Asterisk indicates significance between the Pre- (HC) and Post-BGP-15 (HC+BGP-15) groups (*: $p<0.05$; paired t-test, normal data distribution). HC: hypecholersterolemic, LV: left ventricle

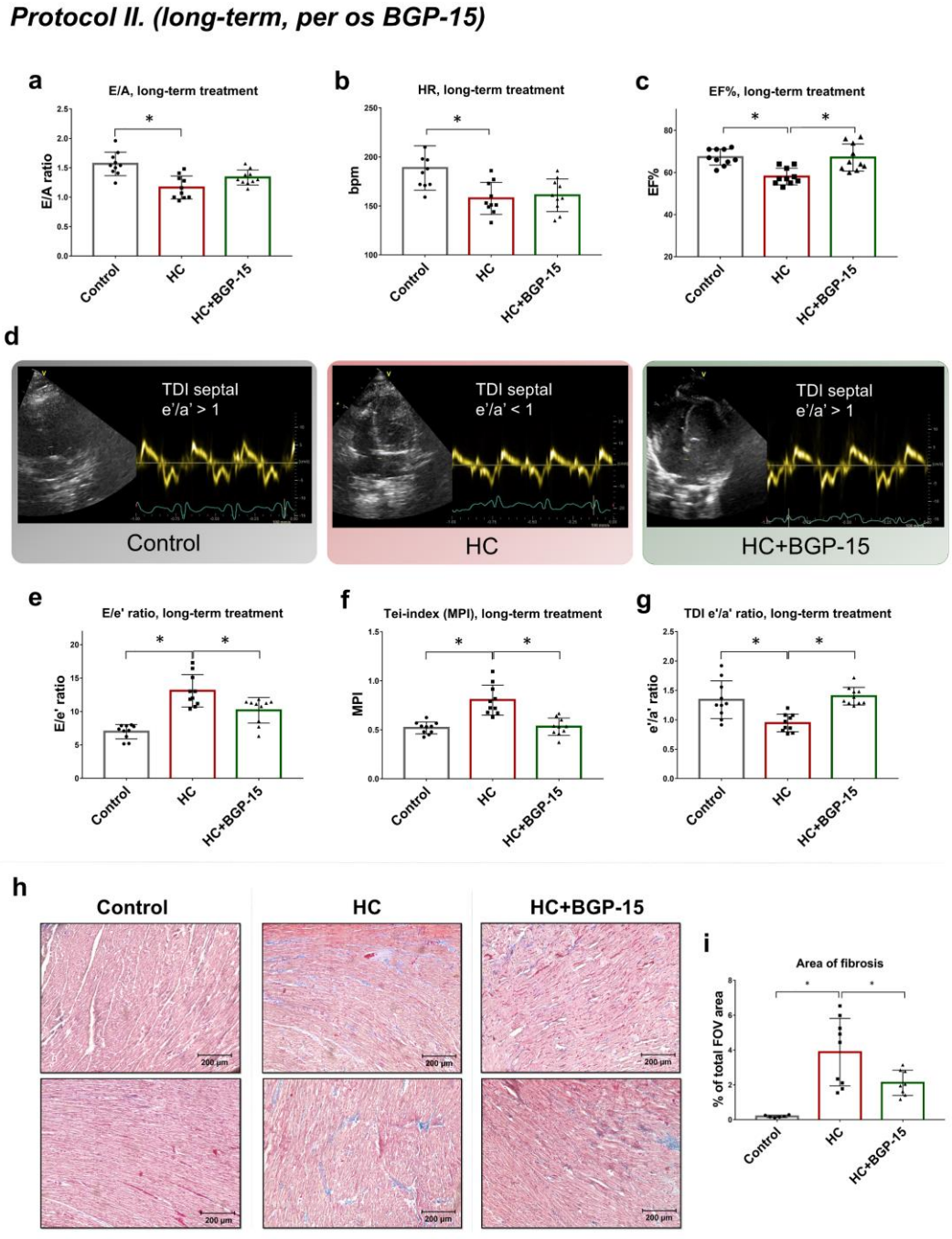


**Figure 3.** Chronic BGP-15-treatment improved the diastolic parameters of HC rabbits. Groups are Control (n=10), HC (n=10) and HC+BGP-15 (n=10). (**a**) Transmitral E/A ratio, (**b**) heart rate (HR) and (**c**) ejection fraction (EF) of rabbits in the 3 study groups of the long-term protocol. (**d**) Original echocardiography traces of tissue Doppler imaging (TDI, apical 4-chamber view) from Control, HC and HC+BGP-15 groups, respectively. All data followed normal distribution. Data presented as mean±SEM, one-way ANOVA with Tukey post-testing. (**e**) E/e' ratio, (**f**) Tei-index and (**g**) tissue Doppler e'/a' ratio improved in the BGP-15 treated group compared to HC. (**h**) Representative images of myocardial tissue samples stained with Masson's trichrome show the fibrotic (blue) areas. Groups are Control (n=6), HC (n=9) and HC+BGP-15 (n=8), respectively. (**i**) Graph shows the area of fibrosis (%) normalized to the total field-of-view (FOV). All data followed normal distribution. Data presented as mean±SEM, one-way ANOVA with Tukey post-testing; *: $p<0.05$. HC: hypercholesterolemic; FOV: field-of-view

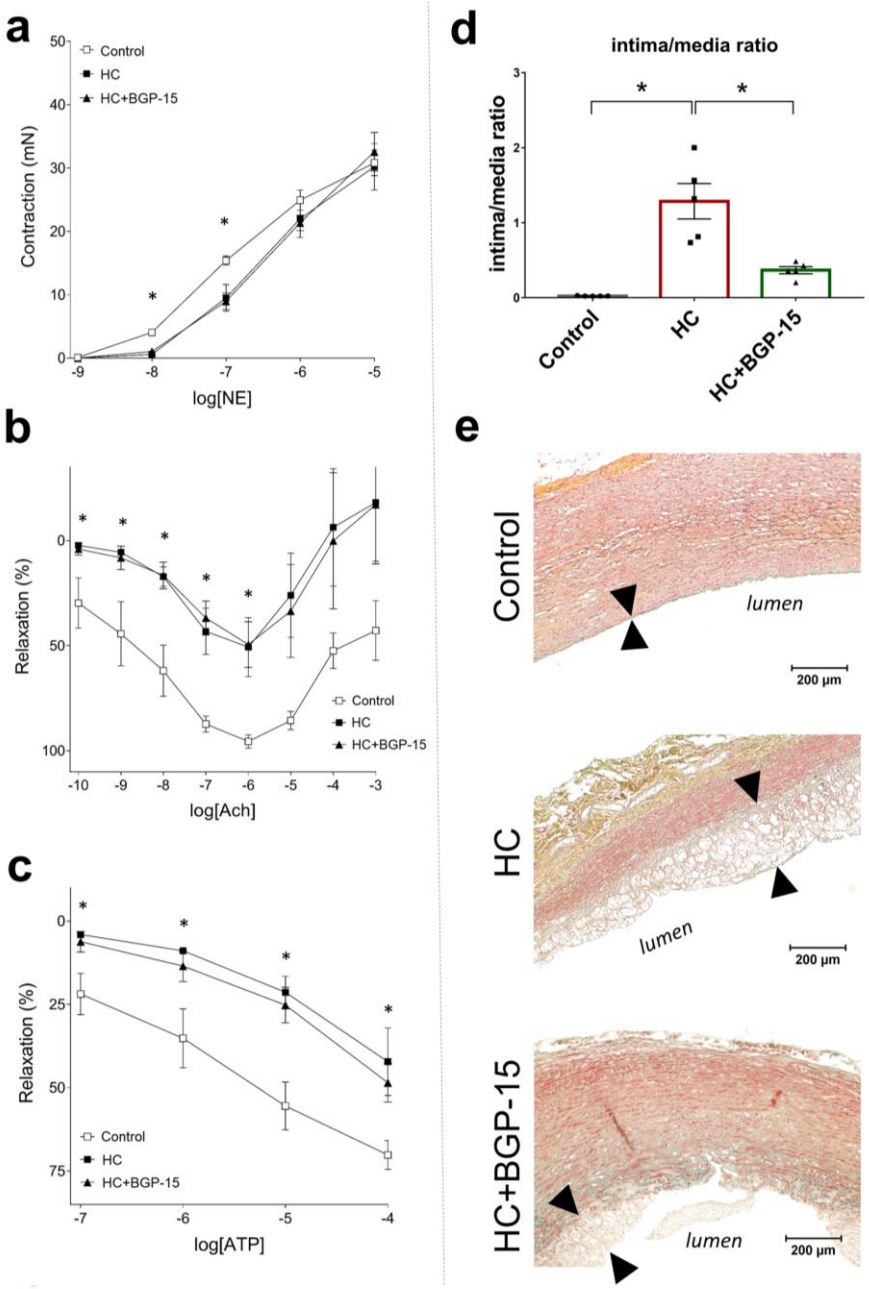


**Figure 4.** Vascular studies of the long-term treatment groups. (**a)** The effect of norepinephrine (NE) on the thoracic aorta. The axis x shows the common logarithm of the NE concentration; axis y indicates the contractile force (over the resting level). (**b**) The effect of acetylcholine (Ach) and (**c**) adenosine-5′-triphosphate (ATP) on the isolated aorta. The axis x shows the common logarithm of the molar concentrations of Ach and ATP, respectively, and the axis y indicates the effect as a percentage decrease in the contractile force. The symbols represent the averaged effects ± SEM (n=5/group); *: $p<0.05$). There was no significant difference in vasorelaxation between HC and HC+BGP-15 groups (one-way ANOVA, Tukey post-test). (**d**) Graph represents averaged intima/media ratios (long-term protocol); normal distribution, mean ± SEM, one-way ANOVA, Tukey post-test, (n=5/group; *: $p<0.05$). (**e**) Representative images of aortic cross-sections from Control, HC and HC+BGP-15 groups, respectively, stained with Movat pentachrome (magnification: 40x). Arrows denote the intimal thickness and atherosclerotic lesion with foam cells. HC: hypercholesterolemic

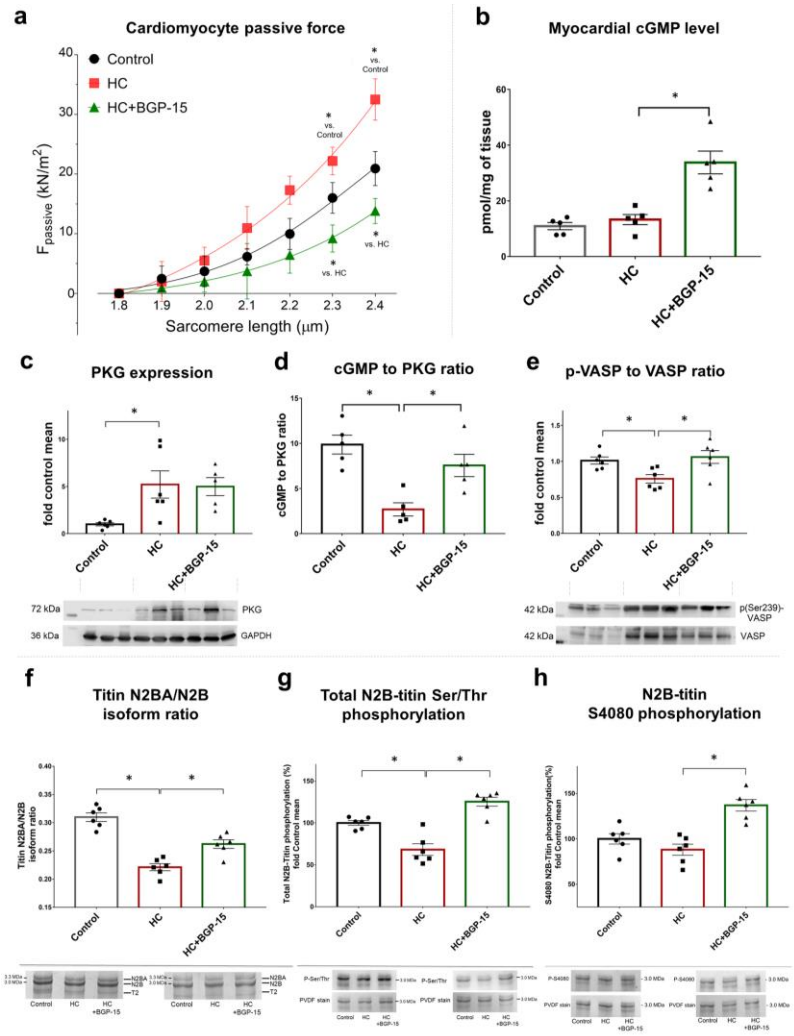


**Figure 5.** BGP-15 reduces myocyte stiffness, increases PKG activity and titin phosphorylation. (**a**) Cardiomyocyte passive force – sarcomere length relations in myocytes of long-term study groups. Myofilament passive force was significantly reduced in the samples of the BGP-15-treated animals compared to HC. Curves are second-order polynomial fits to the means±SEM; (N=5 and n=5/group; *: $p<0.05$). (**b**) Myocardial cGMP level (pmol/mg of tissue) elevated in HC+BGP-15 group compared to HC (n=5/group). (**c**) PKG expression elevated in both HC and HC+BGP-15 groups compared to Control (n=6/group). (**d**) cGMP to PKG ratio diminished in HC samples compared to Control, but elevated in HC+BGP-15 compared to HC (n=5/group). (**e**) Phospho(Ser239)-VASP to VASP ratios in study groups. VASP phosphorylation at Ser239 diminished in HC, but elevated in HC+BGP-15 groups (n=6/group). (**f**) Titin N2BA/N2B isoform ratio was significantly decreased in HC animals compared to Control, and increased in HC+BGP-15 group compared to HC (n=6/group). Insets (bottom) show representative gel stains at molecular weight of ≈ 3.0 MDa (titin N2B isoform) and ≈3.3 MDa (titin N2BA isoform). (**g**) Total titin Ser/Thr phosphorylation (n=6/group), and (**h**) PKG-dependent titin Ser4080 phosphorylation increased in myocardial samples of BGP-15-treated animals compared to HC (n=6/group). Representative images (in **g** and **h** panels) show immunoblots using Ser/Thr phospho-antibody, anti-phospho-S4080 N2B-titin antibody (top panels) and PVDF staining (bottom, used for normalization). All data followed normal distribution (Shapiro-Wilk test). Data presented as mean±SEM, ANOVA, Tukey post-test; *: $p<0.05$ denotes significance. HC: hypercholesterolemic; cGMP: cyclic guanosine monophosphate; PKG: protein kinase G; VASP: vasodilator-stimulated phosphoprotein, Ser: serine, Thr: threonine

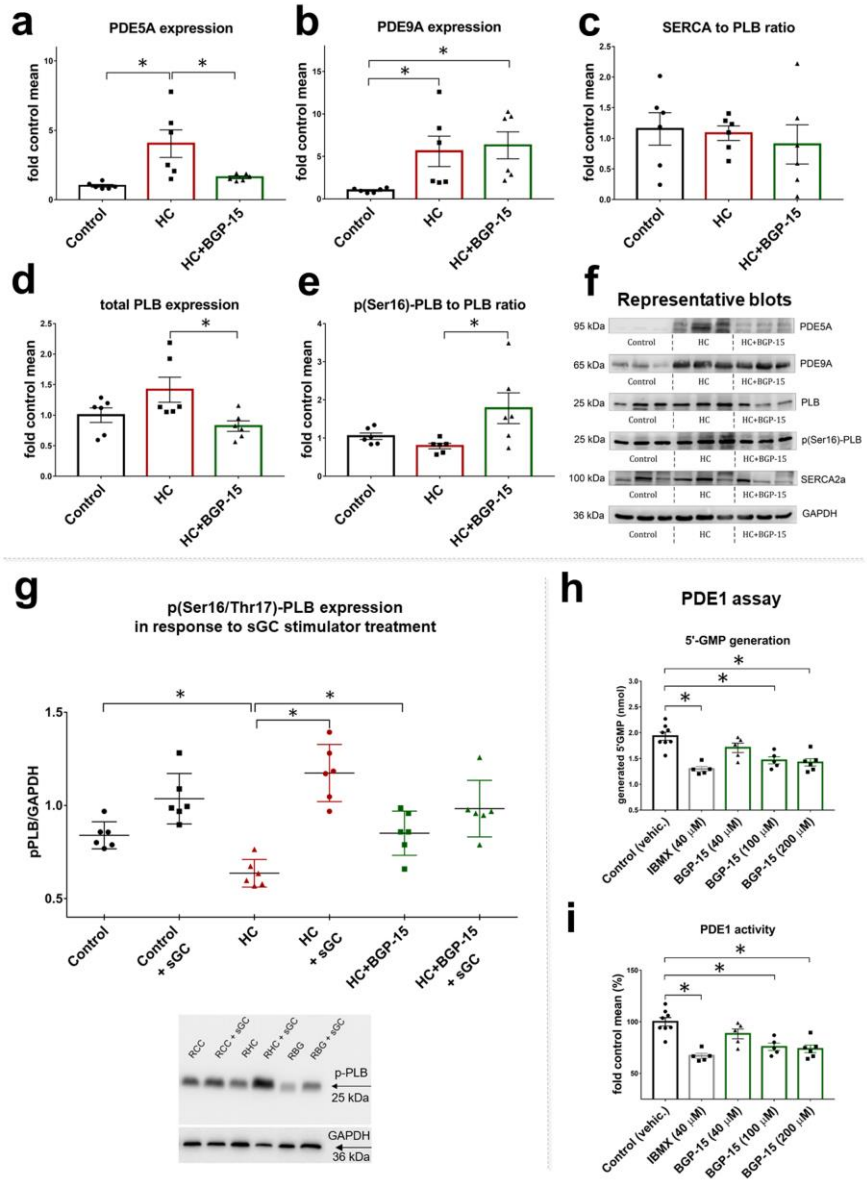


**Figure 6.** BGP-15 decreases PDE expression and activity, and restores PLB phosphorylation. (**a**) Myocardial expression of PDE5A elevated in HC rabbits, but decreased in the LV samples of BGP-15-treated animals (n=6/group, ANOVA, Tukey post-test). (**b**) Myocardial PDE9A expression elevated in both HC and HC+BGP-15 groups compared to Control (n=6/group, Kruskal-Wallis test, Dunn's post hoc test). (**c**) No significant differences were found among treatment groups in SERCA2a to PLB ratio (n=6/group, ANOVA, Tukey post-test). (**d**) Total phospholamban (PLB) expression was diminished in samples of BGP-15-treated animals in comparison to HC (n=6/group, Kruskal-Wallis test, Dunn's post hoc test). (**e**) p(Ser16)-PLB to total PLB ratio. PLB Ser16 phosphorylation increased in HC+BGP-15 group compared to HC (n=6/group, ANOVA, Tukey post-test). (**f**) Representative blots of proteins of interest in left ventricle samples of rabbits. Protein expressions were normalized to GAPDH, and were expressed in the percentage of Control (which was considered 100%). Data presented as mean±SEM; *: $p<0.05$. (**g**) p(Ser16/Thr17)-PLB expression was decreased in HC, but was increased in HC+BGP-15 group (n=6/group; mean±SEM, normal distribution, one-way ANOVA, *: $p<0.05$ denotes significance). Treatment of the samples with an sGC stimulator (BAY 41-2272) could not further increase PLB phosphorylation in Control and HC+BGP-15

groups, but increased PLB phosphorylation in HC samples (mean±SEM, n=6/group; paired t-test between corresponding groups; *: $p<0.05$ denotes significance). Representative blots for p-PLB measurements are shown below. (**h, i**) BGP-15 inhibits phosphodiesterase 1 enzyme activity in vitro. Without inhibition (Control, n=8), 20 mU PDE1 enzyme generated 2 nmoles of 5'GMP from 200 µM cGMP at 37 °C in 60 minutes. A non-specific PDE inhibitor (IBMX 40 µM, n=5) decreased PDE activity. BGP-15 dose-dependently inhibited PDE activity comparably to IBMX, which was significant (compared to Control) in concentrations of 100 µM (n=5) and 200 µM (n=6). Data presented as mean±SEM, data distribution was estimated using Shapiro-Wilks method, data followed normal distribution; one-way ANOVA with Tukey post-test; *: $p<0.05$ denotes significance. sGC: soluble guanylate cyclase, PDE: phosphodiesterase, PLB: phospholamban, SERCA2a: sarco/endoplasmic reticulum $Ca^{2+}$-ATPase, Ser: serine, Thr: Threonine, GMP: guanosine monophosphate

# BGP-15 improves diastolic function in a rabbit model of atherosclerotic cardiomyopathy

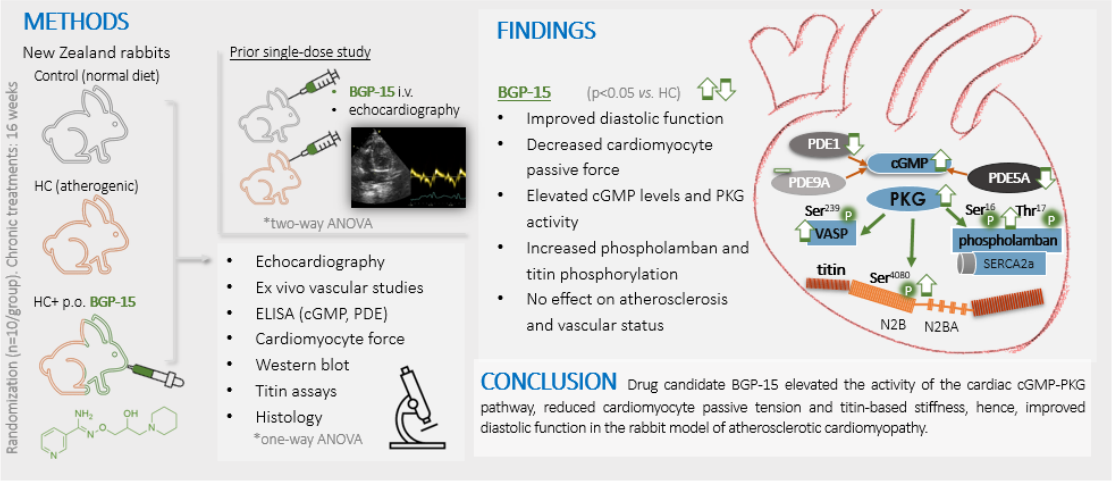


Priksz, et al. *Br. J. Pharmacol.*

BJP British Journal of Pharmacology